THE JOURNAL OF BIOLOGICAL CHEMISTRY VOL. 285, NO. 41, pp. 31647–31660, October 8, 2010
© 2010 by The American Society for Biochemistry and Molecular Biology, Inc. Printed in the U.S.A.

Nucleobindin 1 Is a Calcium-regulated Guanine Nucleotide Dissociation Inhibitor of $G\alpha_{i1}$ *[S]

Received for publication, May 27, 2010 Published, JBC Papers in Press, August 2, 2010, DOI 10.1074/jbc.M110.148429

Neeraj Kapoor[‡1], Ruchi Gupta[‡1], Santosh T. Menon[‡], Ewa Folta-Stogniew[§], Daniel P. Raleigh[¶‖], and Thomas P. Sakmar[‡2]

From the [‡]Laboratory of Biochemistry and Molecular Biology, Rockefeller University, New York, New York 10065, the [§]W. M. Keck Foundation Biotechnology Resource Laboratory, Yale University School of Medicine, New Haven, Connecticut 06520, and the [¶]Department of Chemistry and [‖]Graduate Program in Biochemistry and Structural Biology and Graduate Program in Biophysics, State University of New York, Stony Brook, New York 11794

Nucleobindin 1 (NUCB1) is a widely expressed multidomain calcium-binding protein whose precise physiological and biochemical functions are not well understood. We engineered and heterologously expressed a soluble form of NUCB1 (*s*NUCB1) and characterized its biophysical and biochemical properties. We show that *s*NUCB1 exists as a dimer in solution and that each monomer binds two divalent calcium cations. Calcium binding causes conformational changes in *s*NUCB1 as judged by circular dichroism and fluorescence spectroscopy experiments. Earlier reports suggested that NUCB1 might interact with heterotrimeric G protein α subunits. We show that dimeric calcium-free *s*NUCB1 binds to expressed $G\alpha_{i1}$ and that calcium binding inhibits the interaction. The binding of *s*NUCB1 to $G\alpha_{i1}$ inhibits its basal rate of GDP release and slows its rate and extent of GTPγS uptake. Additionally, our tissue culture experiments show that *s*NUCB1 prevents receptor-mediated $G\alpha_i$-dependent inhibition of adenylyl cyclase. Thus, we conclude that *s*NUCB1 is a calcium-dependent guanine nucleotide dissociation inhibitor (GDI) for $G\alpha_{i1}$. To our knowledge, *s*NUCB1 is the first example of a calcium-dependent GDI for heterotrimeric G proteins. We also show that the mechanism of GDI activity of *s*NUCB1 is unique and does not arise from the consensus GoLoco motif found in RGS proteins. We propose that cytoplasmic NUCB1 might function to regulate heterotrimeric G protein trafficking and G protein-coupled receptor-mediated signal transduction pathways.

Heterotrimeric guanine nucleotide-binding proteins, G proteins, couple to heptahelical cell surface G protein-coupled receptors (GPCRs)[3] and participate in intracellular signaling events. The G protein heterotrimer is composed of the Gα subunit and the G$\beta\gamma$ heterodimer. Upon ligand-mediated activation, GPCRs catalyze the exchange of GDP for GTP on Gα leading to dissociation of the heterotrimer into Gα·GTP and G$\beta\gamma$ subunits (1–3). These individual subunits then regulate downstream signaling cascades involving effector systems like adenylyl cyclases, Ca^{2+} and K^+ channels, phospholipase C isozymes, and cyclic nucleotide phosphodiesterases (4, 5). Thereafter, the intrinsic GTPase activity of Gα reverts it back to the GDP-bound state, which can reassociate with G$\beta\gamma$. This inhibits the interaction of G protein subunits with downstream effectors, which results in the turning-off of the signaling pathways. Hence, signaling by heterotrimeric G proteins is directly dependent on the lifetime of the GTP-bound state of Gα. This lifetime is regulated by GTPase-accelerating proteins (GAPs), which catalyze the rapid hydrolysis of the Gα-bound GTP to GDP and by guanine nucleotide dissociation inhibitors (GDIs), which inhibit the exchange of GDP for GTP in the catalytic pocket of Gα (6).

Together, GAPs and GDIs exert a regulatory control on G protein signaling. In recent years, novel interacting partners of heterotrimeric G proteins called the regulators of G protein signaling or RGS proteins have been discovered that possess GAP activity (7, 8). Interestingly, RGS12 and RGS14 in addition to functioning as GAPs can also act as GDIs (9, 10). In 1999, Lanier and co-workers (11) used yeast two-hybrid analysis to identify distinct receptor-independent activators of G protein signaling or AGS proteins. Several members of this AGS family (AGS3-6) have been shown to function as GDIs of $G\alpha_i$ subunits (12). The observed GDI activity of both AGS and RGS proteins toward $G\alpha_{i/o}$ is attributed to a 19-amino acid consensus sequence called the GoLoco motif (9, 13, 14). Earlier in 1995, in an independent yeast two-hybrid screen, Mochizuki *et al.* (15) established the interaction of a novel Golgi-resident Ca^{2+}-binding protein Nucleobindin 1 or NUCB1, specifically with the heterotrimeric G protein α subunit, $G\alpha_{i2}$. Subsequently, Lin *et al.* (16) demonstrated that NUCB1 interacts exclusively with the adenylyl cyclase inhibitory ($G\alpha_i$) and stimulatory ($G\alpha_s$) classes of Gα subunits. In a recent study, it was shown that overexpression of NUCB1 causes redistribution of only the $G\alpha_{i1}$ subunits and not the G$\beta\gamma$ subunits to the plasma membrane and regulated secretion granules (17). However, a role for NUCB1 in modulating $G\alpha_{i1}$ activation and the biochemistry of NUCB1-$G\alpha_{i1}$ interaction has not been reported.

* This work was supported, in whole or in part, by National Institutes of Health Grant GM078114. This work was also supported by Rockefeller/Sloan-Kettering/Weill Cornell Tri-Institutional Training Program in Chemical Biology.

[S] The on-line version of this article (available at http://www.jbc.org) contains supplemental Figs. S1–S7.

[1] Both authors contributed equally to this work.

[2] To whom correspondence should be addressed. Tel.: 212-327-8284; Fax: 212-327-7904; E-mail: sakmar@mail.rockefeller.edu.

[3] The abbreviations used are: GPCR, G protein-coupled receptor; GTPγS, guanosine 5′-3-*O*-(thio)triphosphate; GDI, guanine nucleotide dissociation inhibitor; AC, adenylyl cyclase; GAP, GTPase-accelerating protein; DLS, dynamic light scattering; MALS, multiangle light scattering; SEC, size-exclusion chromatography; AUC, analytical ultracentrifugation; mGTPγS, mant(2′,3′-*O*-(*N*-methyl-anthraniloyl)-GTPγS; ITC, isothermal titration calorimetry; RI, refractive index; LS, light scattering.

NUCB1 is a 55-kDa multidomain Ca^{2+}-binding protein that was first identified as a novel B cell growth and differentiation factor associated with lupus syndrome (18). NUCB1 derives its trivial name, Calnuc, from its Ca^{2+}-binding and DNA-binding ability (19). The DNA-binding domain of basic residues (172–218) lies at the N terminus following the signal sequence. The Ca^{2+}-binding domain is at the core of the protein sequence consisting of two EF hand motifs with an intervening acidic region (residues 253–316). The Ca^{2+}-binding domain is followed by a leucine zipper domain (residues 347–389), which has been postulated to induce NUCB1 dimerization (Fig. 1*A*) (20). The C-terminal (*CT*) region following the leucine zipper domain is predicted to be intrinsically disordered and unstructured. Intriguingly, NUCB1 is strongly conserved from flies to humans (21) and is widely distributed among Golgi (16, 22), nucleus (19, 23), endoplasmic reticulum (24, 25), and cytoplasm (17). The N-terminal signal sequence of NUCB1 targets it to different membrane compartments and its deletion renders NUCB1 cytosolic.

Recently, Brodeur *et al.* (26) reported the role of NUCB1 in LDL receptor-related protein 9 (LRP9) trafficking where the cytosolic NUCB1 fraction helps in LRP9 endosomal sorting and prevents its delivery to lysosomes. The ubiquitous expression of NUCB1 in various cell and tissue types results in a diverse interactome, including interacting partners like G protein α subunits, cyclooxygenases, and amyloid precursor protein (16, 25–27). Several classes of $G\alpha$ subunits have been shown to interact with NUCB1 (16, 25–27). Yeast two-hybrid experiments performed with various deletion constructs of either $G\alpha_{i3}$ or NUCB1 mapped the C-terminal α5 helix domain of the G protein and the acidic region of NUCB1 (residues 264–305) to be necessary for interaction (28). Immunofluorescence-based studies showed that NUCB1 and $G\alpha_i$ protein subunits co-localize on the Golgi lumen and regulated secretion granules (17). Because $G\alpha$ subunits are ubiquitously involved in numerous signal transduction pathways in different tissue types, their interaction with NUCB1 might regulate downstream signaling events.

We are interested in understanding the role of the α5 helix of the G protein α subunit in regulating nucleotide exchange rates (29–31). Because the α5 helix of $G\alpha$ is involved in interaction with NUCB1, we characterized and studied the interaction of NUCB1 with $G\alpha_{i1}$ in detail. In this study, we present the detailed biophysical and biochemical characterization of the Ca^{2+}-binding ability and the oligomeric state of a heterologously expressed N-terminally truncated soluble form of NUCB1, termed *s*NUCB1 (Fig. 1*A*). We show that *s*NUCB1 binds Ca^{2+} and exists as a dimer in solution. Ca^{2+}-free *s*NUCB1 preferentially binds $G\alpha_{i1}$ and inhibits its GDP release as demonstrated by several independent assays. We have shown that overexpression of *s*NUCB1 in HEK293 cells markedly decreases ligand-dependent receptor-mediated $G\alpha_i$ inhibition of adenylyl cyclase. We conclude that *s*NUCB1 serves as a novel Ca^{2+}-regulated GDI of $G\alpha_{i1}$. Our findings suggest that NUCB1 is involved in regulating cytoplasmic G protein signaling pathways.

EXPERIMENTAL PROCEDURES

Reagents

GDP sodium salt and GTPγS tetralithium salt were purchased from Sigma. The fluorescent GTPγS analogue, mant(2′,3′-*O*-(*N*-methyl-anthraniloyl)-GTPγS was purchased from Jena Biosciences (Jena, Germany), and BODIPY-FL-GTPγS was purchased from Molecular Probes (Invitrogen). The His_6-tagged mutants of WT $G\alpha_{i1}$ were generated by site-directed mutagenesis using the high fidelity thermostable DNA polymerase *Pfu* (Stratagene). The cAMP dynamic 2 kit was purchased from CisBio (Bedford, MA) for cell-based studies. All reagents and chemicals used were of highest available purity.

Heterologous Expression of sNUCB1 and Heterotrimeric G Protein α-Subunit $G\alpha_{i1}$

The cDNA clones for human NUCB1 and rat $G\alpha_{i1}$ were obtained from the ATCC. The DNA fragment for the soluble form of NUCB1 or *s*NUCB1, corresponding to residues 31–461 of the human NUCB1 protein without the N-terminal signal sequence (residues 1–31), was cloned into the pET28a(+) expression vector (Amersham Biosciences). Similarly, the DNA fragment corresponding to full-length WT rat $G\alpha_{i1}$ subunit (residues 1–354) was cloned into the pET28a(+) expression vector. The vector was used to transform BL21 (DE3) cells to express an N-terminal His_6 tag protein containing a PreScission protease site directly after the His_6 tag. The expressed construct for *s*NUCB1 served as a template for introducing site-specific mutations using the QuikChange system (Stratagene, La Jolla, CA) to generate *s*NUCB1(W232A/W333A) or for introducing a missense mutation to generate the truncated version of the protein, namely *s*NUCB1(W333Ter). All proteins were expressed in BL21 (DE3) cells grown in the presence of 50 μg/ml kanamycin. Cells were grown at 37 °C to $A_{600\ nm}$ of ~0.7 and then induced with 500 μM isopropyl 1-thio-β-D-galactopyranoside (United States Biological). Post-induction, the culture was grown overnight at 17 °C and subsequently harvested. The resulting pellets were resuspended in a buffer containing 50 mM Tris-HCl, pH 8.0, 150 mM NaCl, 50 mM β-mercaptoethanol, bovine lung aprotinin (20 mg/ml), 2 mM phenylmethanesulfonyl fluoride (PMSF), and complete EDTA-free protease inhibitor mixture tablets (Roche Applied Science). Thereafter, the cells were lysed, and the expressed His_6 tag protein was purified from crude extract by affinity chromatography using nickel-nitrilotriacetic acid column pre-equilibrated with buffer A (50 mM Tris, pH 8.0, 150 mM NaCl, 50 mM β-mercaptoethanol) for *s*NUCB1 and its variants and buffer A′ (50 mM Tris, pH 8.0, 150 mM NaCl, 2 mM $MgCl_2 \cdot 6H_2O$, 10 μM GDP, 50 mM β-mercaptoethanol) for WT $G\alpha_{i1}$. The bound His_6 tag protein was eluted from the column by using buffer A or buffer A′ supplemented with 500 mM imidazole. The His_6 tag was cleaved by PreScission™ protease, which was subsequently removed. To remove Ca^{2+} from *s*NUCB1 or its variants, the proteins were extensively dialyzed against buffer A supplemented with 5 mM EGTA and 1 mM EDTA, which are also eventually removed through dialysis. Finally, SEC was done using a Superdex200 26/60 HR column equilibrated with buffer S (50 mM Tris, pH 8.0, 150 mM NaCl) for *s*NUCB1 and its variants and equilibrated in buffer S′ (50

mM Tris, pH 8.0, 150 mM NaCl, 2 mM $MgCl_2 \cdot 6H_2O$, 10 μM GDP, 1 mM DTT) for WT $G\alpha_{i1}$ to obtain homogeneously pure protein. The typical yield for *s*NUCB1 and its variants was ~5 mg/liter and for WT $G\alpha_{i1}$ ~12–15 mg/liter. The purity of the proteins was assessed by Coomassie Brilliant Blue staining after the proteins were separated through SDS-PAGE. The purity of all proteins was greater than 95%.

Isothermal Titration Calorimetry (ITC)

ITC was performed at 25 °C (298 K) using a MicroCal VP-ITC (MicroCal, Northhampton, MA) calorimeter. To measure quantitatively the binding of Ca^{2+} or WT $G\alpha_{i1}$·GDP to *s*NUCB1, 2 ml of 50 μM *s*NUCB1 (Ca^{2+}-free) and 700 μl of either 500 μM $CaCl_2 \cdot 6H_2O$ (prepared in 50 mM Tris, pH 8.0, 150 mM NaCl) or 600 μM WT $G\alpha_{i1}$·GDP (prepared in 50 mM Tris, pH 8.0, 150 mM NaCl, 2 mM $MgCl_2 \cdot 6H_2O$, 10 μM GDP, 1 mM tris(2-carboxyethyl)phosphine) was used and thoroughly degassed. Contents of the sample cell were stirred continuously at 280 rpm during the experiment. A typical titration of *s*NUCB1 involved 50 injections each of 5 μl of $CaCl_2 \cdot 6H_2O$ (500 μM) or WT $G\alpha_{i1}$·GDP (600 μM) into a sample cell containing 1.4 ml of *s*NUCB1 (50 μM). The heat of dilution of the titrant ($CaCl_2 \cdot 6H_2O$ or WT $G\alpha_{i1}$·GDP) was subtracted from the titration data for base-line correction. The base line-corrected data were analyzed with MicroCal Origin™ 6.0 software to determine the change in enthalpy (ΔH) and association constant (K_a). Thermal titration data fit showed two sets of binding sites for Ca^{2+} to *s*NUBC1. The parameters were calculated based on three or more independent titration experiments. Each numerical value reported is the mean ± S.E. among the independent data sets.

Size-exclusion Chromatography

Complex Formation between sNUCB1 and WT $G\alpha_{i1}$—Complex formation between *s*NUCB1 and $G\alpha_{i1}$ was monitored using SEC. 150 μM *s*NUCB1 ($-Ca^{2+}/+Ca^{2+}$) was incubated with 256 μM $G\alpha_{i1}$·(GDP/GTPγS) in 20 mM Tris, pH 8.0, 100 mM NaCl, 10 mM $MgCl_2$, 10 μM GDP, and 1 mM DTT at 30 °C for 20 min with minimal shaking to enable saturation binding. WT $G\alpha_{i1}$ in the GTPγS-bound state was generated by incubating WT $G\alpha_{i1}$·GDP with 5 mM GTPγS for 30 min at 30 °C to ensure complete exchange of nucleotide. Furthermore, the complete exchange was confirmed by the AlF_4^- exchange assay. About 200 μl of the reaction mixture was injected onto Superdex200 10/30 GL column attached to AKTA FPLC (GE Healthcare) and run at 4 °C. Elution was done with the incubation buffer at a flow rate of 0.5 ml/min with 0.35-ml fractions collected. Peak fractions were analyzed through SDS-PAGE and Coomassie-stained to analyze the complex formation.

Estimation of sNUCB1 Molecular Mass Using Heavy Molecular Weight Standards—Purified *s*NUCB1 or the heavy molecular weight standards (GE Healthcare) were injected onto a Superdex200 10/30 GL column pre-equilibrated with buffer S, and the normalized absorbance of the eluting peak was plotted. A calibration curve of K_{av} ($V_e - V_o/V_c - V_o$) *versus* $\log_{10}$(molecular weight) was plotted, where V_e is the elution volume; V_o is the column void volume corresponding to the elution of blue dextran, and V_c is the geometric column volume. The data were fit to a straight line curve like $Y = A + Bx$, where $A = 1.915$ and $B = 0.311$ were obtained from the fit. Therefore, for a $Y = K_{av}$ value, the corresponding value of $\log_{10}$ (molecular weight) was obtained to estimate the molecular mass of *s*NUCB1 and *s*NUCB1(W333Ter).

Light Scattering

Multiangle Light Scattering (MALS) and Dynamic Light Scattering (DLS)—The light scattering data were collected using a Superdex200 10/30, HR SEC column (GE Healthcare), connected to an HPLC system (Agilent 1200, Agilent Technologies, Wilmington, DE) equipped with an autosampler. The elution from SEC was monitored by a photodiode array UV-visible detector (Agilent Technologies), differential refractometer (OPT-Lab rEx, Wyatt Corp., Santa Barbara, CA), static and dynamic, multiangle laser light scattering detector (HELEOS II with QELS capability, Wyatt Corp.). The SEC-UV/LS/RI system was equilibrated in buffer (50 mM Tris, pH 8.0, 150 mM NaCl) for *s*NUCB1 alone and in buffer (50 mM Tris, pH 8.0, 100 mM NaCl, 10 mM $MgCl_2$, 10 μM GDP, 1 mM DTT) for WT and truncated *s*NUCB1/G protein complex at the flow rate of 1.0 ml/min. Two software packages were used for data collection and analysis; the Chemstation software (Agilent Technologies) controlled the HPLC operation and data collection from the multiwavelength UV-visible detector, and the ASTRA software (Wyatt Corp., Santa Barbara, CA) collected data from the RI detector and the LS detectors and recorded the UV trace at 280 nm sent from the photodiode array detector. The weight average molecular masses, M_w, were determined across the entire elution profile in the intervals of 1 s from static LS measurement using ASTRA software as described previously (32). The approach uses a Rayleigh-Debye-Gans light scattering model (Equation 1), which relates the amount of scattered light to the concentration and weight average molecular weight of solute and second virial coefficient,

$$\frac{K^*c}{R(\theta)} = \frac{1}{\bar{M}_w} + 2A_2c \qquad \text{(Eq. 1)}$$

where $R(\theta)$ is the intensity of excess scattered light at angle θ; c is the concentration of the solute, $\bar{M}_w$ is the weight average molecular weight of the solute; A_2 is the second virial coefficient; K^* is an optical parameter equal to $4\pi^2n^2 (dn/dc)^2/(\lambda_0^4 N_A)$, where n is the refractive index; dn/dc is the refractive index increment for the solute; N_A is Avogadro's number, and λ_0 is the wavelength of the scattered light.

DLS measurements were made "on line" at an angle of 100° with a 2-s collection time. Time-resolved scatter intensity fluctuations were analyzed using Astra software (Wyatt Corp.), which implements the cumulants method (33) to determine the time dependence of diffusive motion also referred to as the intensity correlation function, $G(T)$, as shown in Equation 2 (34),

$$G(T) = B\{1 + \alpha(\exp(-D_T q^2 t))^2\} \qquad \text{(Eq. 2)}$$

where B is the average base-line intensity; α is an instrument-specific correction factor; D_T is the concentration-dependent translational diffusion constant of the solute; t is a delay time,

and q is the scattering vector equal to $(4\pi n)/\lambda \sin\theta/2$, where n is the refractive index of the solvent; λ is the wavelength of the scattered light, and θ is the scattering angle. Equation 2 describes the relationship between the time dependence of fluctuation in scatter intensity and the translational diffusion coefficient. The value of D_T can be used to estimate the apparent hydrodynamic radius of an equivalent sphere using Stokes-Einstein relationship shown in Equation 3,

$$R_h = \frac{kT}{6\pi\eta D_T} \quad \text{(Eq. 3)}$$

where k is the Boltzmann constant; T is the absolute temperature, and η is the temperature-corrected viscosity of the solution.

Determination of Dimerization Equilibrium Constant from SEC-UV/LS/RI—The concentration-dependent changes in the weight average molecular mass determined for the apex of the eluting peak for *s*NUBC1 were used to determine the dimerization constant. The weight average molecular weights were plotted as a function of protein concentration for *s*NUCB1; error bars represent ±3% of $\bar{M}_w$ for concentrations above 100 μg/ml, ±5% of $\bar{M}_w$ for concentrations between 1 and 100 μg/ml, and ±10% of the $\bar{M}_w$ for concentrations below 1 μg/ml. Lines represent the nonlinear least square fits to a monomer-dimer association model for *s*NUCB1 dimerization.

Determination of K_d of Complex Formation from SEC-UV/LS/RI—The concentration-dependent changes in the $\bar{M}_w$ determined for the apex of the eluting peak were used to determine the complexation of Gα$_{i1}$ with *s*NUCB1/*s*NUCB1(W333Ter). The $\bar{M}_w$ values were plotted as a function of total protein concentration for complexation; error bars represent ±3% of $\bar{M}_w$ for concentrations above 100 μg/ml, ±5% of $\bar{M}_w$ for concentrations between 1 and 100 μg/ml, and ±10% of $\bar{M}_w$ for concentrations below 1 μg/ml. Lines represent the nonlinear least square fits to a stimulated complexation model using Origin 6.0.

Fluorescence Spectroscopy

Steady-state Trp Fluorescence upon Ca^{2+} Binding—Steady-state fluorescence measurements for *s*NUCB1 were carried out in a SPEX τ3 spectrofluorimeter (Jobin-Yvon Instruments) at 25 °C. The excitation wavelength was set at 295 nm, although emission spectra were collected from 310 to 460 nm. The excitation and emission slit widths were 2.5 and 5.0 nm, respectively. 178 nM Ca^{2+}-free *s*NUCB1 equilibrated in buffer containing 50 mM Tris, pH 8.0, 100 mM NaCl was incubated with increasing concentrations of Ca^{2+} with constant stirring for 5 min. Thereafter, Trp emission fluorescence spectra were collected for each concentration of Ca^{2+} added.

Quenching of Tryptophan Fluorescence by Small Molecule Quenchers—The excitation wavelength was set at 295 nm, and the emission spectra were collected from 315 to 460 nm with the excitation slit and emission slit width being 2.5 and 5 nm, respectively. 333 nM of protein was equilibrated in buffer containing 50 mM Tris, pH 8.0, and 100 mM NaCl. To study the interaction between the protein and the quenchers, small aliquots of the quenchers were added incrementally from a concentrated stock solution. In the case of potassium iodide, a small quantity of $Na_2S_2O_3$ (0.1 mM) was added to prevent it from forming free triiodide (I_3^-). The accessibility of Trp was monitored by analyzing the quenching data using the Stern-Volmer Equation 4,

$$F_0/F = 1 + K_{SV}[Q] \quad \text{(Eq. 4)}$$

where F_0 and F are the fluorescence intensities in the absence and presence of quenchers, respectively; $[Q]$ is the concentration of the quenching molecules, and K_{SV} is the Stern-Volmer quenching constant. In the case of purely collisional quenching mechanism, the Stern-Volmer plot of F_0/F *versus* $[Q]$ is linear with a slope equal to K_{SV}.

Fluorescence-based mant-GTPγS (mGTPγS) Binding Assays—Steady-state fluorescence measurements experiments were carried out in a SPEX τ3 spectrofluorimeter (Jobin-Yvon Instruments) at 25 °C. 15 μM WT Gα$_{i1}$ was incubated with 50 μM *s*NUCB1(W232A/W333A) in the reaction buffer (50 mM Tris-HCl, pH 8.0, 150 mM NaCl, 2 mM $MgCl_2$, and 1 mM DTT) for 5 min with constant stirring. Thereafter, mGTPγS (15 μM) was added to the reaction mixture. FRET was monitored by exciting the intrinsic Trp fluorescence at 295 nm and measuring the fluorescence emission from 310 to 540 nm. In all cases, blank spectra containing buffer with *s*NUCB1(W232A/W333A) alone were subtracted from the final spectra.

Time-based Fluorescence Assays

Time-based fluorescence measurements were performed in a SPEX Fluorolog-2 spectrofluorometer (SPEX Industries, Edison, NJ) at 25 °C. The excitation wavelength was set at 295 nm specifically for Trp residues, although emission wavelength was set at 340 nm. The excitation and emission slit width were 5 nm each.

AlF_4^- Uptake Assay—WT Gα$_{i1}$ was incubated at 25 °C in reaction buffer K (50 mM Tris-HCl, pH 8.0, 150 mM NaCl, 2 mM $MgCl_2$, and 1 mM DTT) with increasing amounts of *s*NUCB1(W232A/W333A) for 10 min with constant stirring. Thereafter, for AlF_4^--dependent activation of Gα$_{i1}$, a premixed solution of $AlCl_3^-$ (20 mM) and NaF (1 M), respectively, was injected at 180 s. A time course of enhancement in Trp fluorescence coupled to activation was monitored in the presence of increasing concentrations of *s*NUCB1(W232A/W333A) in the reaction mixture.

GTPγS Nucleotide Exchange Assay—WT Gα$_{i1}$ was incubated at 25 °C with increasing concentrations of *s*NUCB1(W232A/W333A) in reaction buffer K for 10 min with constant stirring. The base-line fluorescence was monitored for 200 s after which GTPγS (20 μM) was injected into the reaction mixture, and the relative increase in intrinsic Trp fluorescence (λ_{ex} = 295 nm, λ_{em} = 340 nm) was measured as a function of time for each concentration of *s*NUCB1(W232A/W333A).

BODIPY-FL-GTPγS Nucleotide Exchange Assay—WT Gα$_{i1}$ (20 μM) was incubated at 25 °C in reaction buffer K with increasing concentrations of Ca^{2+}-free *s*NUCB1 for 10 min with constant stirring. BODIPY-FL-GTPγS (20 μM) was added to the reaction mixture, and the relative increase in intrinsic fluorescence (λ_{ex} = 485 nm, λ_{em} = 512 nm) was measured for each concentration of Ca^{2+}-free *s*NUCB1 as a function of time.

BODIPY-FL-GTPγS Nucleotide Binding Assay—WT $G\alpha_{i1}$ (20 μM) was incubated alone and with Ca^{2+}-free *s*NUCB1 (100 μM) at room temperature in reaction buffer K. 10-μl samples were withdrawn from each reaction mixture at various time points and loaded onto a pre-equilibrated Zeba™ micro-desalt spin column to remove the unbound nucleotide. The columns were spun at 1000 × *g* for 1 min, and the flow-through was collected. The amount of bound nucleotide in each flow-through was measured by using BODIPY absorbance at 504 nm (ϵ = 80,000 M^{-1} cm^{-1}). The absorbance at 280 nm was also monitored to ensure that the same amount of protein was being collected in each flow-through sample.

Radioligand [^{35}S]GTPγS-based Nucleotide Exchange Assay

The effect of Ca^{2+}-free *s*NUCB1 or Ca^{2+}-free *s*NUCB1-(W333Ter) binding to WT $G\alpha_{i1}$·GDP on the nucleotide exchange was monitored using [^{35}S]GTPγS exchange assay. 20 μM WT $G\alpha_{i1}$·GDP alone or with 100 μM Ca^{2+}-free *s*NUCB1/*s*NUCB1(W333Ter) was incubated in buffer (10 mM Tris, pH 7.5, 100 mM NaCl, 2 mM $MgCl_2$, 2 mM DTT) for 20 min at 30 °C. After incubation, [^{35}S]GTPγS solution diluted with GTPγS was added to the reaction mixtures such that the final GTPγS concentration in each reaction mixture was 100 μM with an associated radioactivity of 50 nCi/8 μl of reaction volume. Thereafter, 8-μl samples (50 nCi) were withdrawn from each reaction mixture and added to buffer-equilibrated nitrocellulose filters. Subsequently, the filters were extensively washed with Wash buffer (50 mM Tris, pH 7.5, 5 mM $MgCl_2$) to remove excess radioligand. For data analysis, the counts were recorded, and the value for buffer alone was subtracted from each reading. Each individual data point was scaled to the value of radioactivity within 8 μl of reaction volume to get the picomoles of radioligand bound to WT $G\alpha_{i1}$ in each reaction. As a positive control, the C-terminal GoLoco motif peptide from RGS14, namely R14GL(496–531), was used in an identical experimental setup.

Circular Dichroism Spectroscopy

Wavelength Scan—All CD experiments were performed using an Aviv 62A DS CD spectrophotometer. Far-UV CD spectra were recorded at the end of each kinetic run. Spectra were recorded over the wavelength range of 190–250 nm at 1-nm intervals with an averaging time of 3 s using a 0.1-cm path length cell. Background spectrum was subtracted from each of the collected data sets. Each spectrum obtained was an average of three scans. The recorded spectra in millidegrees of ellipticity was converted to mean residue ellipticity in degrees·cm^2 $dmol^{-1}$ using Equation 5,

$$[\theta] = \frac{\theta}{10 \times c \times l \times n} \quad \text{(Eq. 5)}$$

where $[\theta]$ is the mean residue ellipticity in degrees cm^2 $dmol^{-1}$; θ is the ellipticity in millidegrees; *c* is the concentration in M; *l* is the path length in cm, and *n* is the number of peptide bonds.

Thermal Unfolding—The unfolding of the protein (8 μM) with temperature was monitored using CD at a wavelength of 222 nm, which is characteristic of an α-helix. The data points were averaged over 30 s for every unit increment in temperature. A plot of CD signal *versus* temperature was fit to Equations 6 and 7,

$$f(T) = \frac{\alpha_N + \beta_N \times T + (\alpha_D + \beta_D \times T) \cdot e^{\frac{-\Delta G^o_{D-N}(T)}{RT}}}{1 + e^{\frac{-\Delta G^o_{D-N}(T)}{RT}}} \quad \text{(Eq. 6)}$$

where,

$$-\Delta G^o_{D-N}(T) = -\Delta H^o_{D-N}(T_m) * \left(1 - \frac{T}{T_m}\right) - \Delta C^o_P * \left\{(T_m - T) + T * \ln\frac{T}{T_m}\right\} \quad \text{(Eq. 7)}$$

where $f(T)$ is the signal as a function of temperature; T is the temperature; R is the gas constant; α_N defines the intercept; β_N is the slope of the post-transition region of the curve; α_D defines the intercept; β_D is the slope of the pre-transition region of the curve; ΔG^0 is the free energy change for the unfolding reaction; $\Delta H^o_{D\text{-}N}$ is the change in enthalpy for unfolding at the T_m, and ΔC^o_p is the change in heat capacity. Using the above expressions, T_m, the mid-point transition temperature, was estimated along with the change in enthalpy $\Delta H^o_{D\text{-}N}$, for the unfolding reaction at that T_m.

Analytical Ultracentrifugation (AUC)

Sedimentation equilibrium studies were carried out at different centrifugal speeds and protein concentrations for *s*NUCB1 and *s*NUCB1(W333Ter). AUC experiments for *s*NUCB1 (−/+Ca^{2+}) were done at 25 °C with protein concentrations of 50, 100, and 150 μM each at speeds of 20,000, 30,000, and 40,000 rpm. Similarly for *s*NUCB1(W333Ter), AUC experiments were done with 32, 70, and 150 μM protein concentrations each at speeds of 25,000, 30,000, and 40,000 rpm. The individual protein samples were run for sufficiently long periods of time to allow for the equilibrium to generate a time invariant concentration gradient balanced by diffusion of the macromolecular species. The speeds were decided based on the molecular weight of the protein. Under no net transport conditions, the following correlation (Equations 8 and 9) should be observed between concentration and the radial distance (35),

$$Cr = Cr_o * e^{\frac{(\sigma * r)}{2}(r^2 - r_o^2)} \quad \text{(Eq. 8)}$$

where,

$$\sigma = M(1 - \nu\rho) * \frac{\omega^2}{RT} \quad \text{(Eq. 9)}$$

Cr is the concentration of macrosolute at any radial distance r; Cr_o is the concentration of the macrosolute at the reference radial distance r_o; ν is the partial specific volume; ω is the angular velocity; ρ is the density; R is the gas constant; T is the absolute temperature; and M is the molecular mass. The data were analyzed using Optima™ XL-A/XL-I data analysis software (Beckman, 2001).

Western Blot

HEK293 cells were maintained in Dulbecco's modified Eagle medium (Invitrogen) with 10% (v/v) fetal bovine serum (FBS) at 37 °C and 5% CO_2. For Western blot analysis, cells were plated in 6-well plates and transiently transfected with 4 μg of total DNA (3.0 μg of pcDNA3.1(+) + 1.0 μg of WT $G\alpha_{i1}$/*s*NUCB1/CXCR4), and cells were harvested after 48 h. Thereafter, cells were lysed, and the heat-denatured supernatant was subjected to SDS-PAGE analysis. Subsequently, the separated protein fractions were transferred to a PVDF membrane using semi-dry transfer procedures and probed with either 1D4 antibody to detect CXCR4, which has a C-terminal 1D4 tag, or with the respective primary antibodies for NUCB1 or $G\alpha_{i1}$. Finally, the excess antibody was washed away, and the membrane was probed with a horseradish peroxidase-conjugated secondary antibody, and the chemiluminescence upon addition of the substrate was recorded.

cAMP Assay

cAMP dynamic2 assay kit was purchased from CisBio. HEK293 cells (ATCC) were maintained in Dulbecco's modified Eagle's medium (Invitrogen) with 10% (v/v) fetal calf serum (FCS) at 37 °C and 5% CO_2. For cAMP assay, 800,000 cells were plated in a 6-well plate and transiently transfected with pcDNA3.1(+) control, WT $G\alpha_{i1}$, *s*NUCB1, or CXCR4 expression constructs using Lipofectamine 2000 (Invitrogen). Briefly, 4.0 μg of total DNA (3.0 μg of pcDNA3.1(+) + 1.0 μg of WT $G\alpha_{i1}$/*s*NUCB1/CXCR4) was complexed with 12 μl of Lipofectamine 2000 reagent and incubated for 20 min at room temperature before addition of the DNA/lipid mixture to the cells. Cells were plated 24 h after transfection at a density of 8000 cells/well in a poly-D-lysine-coated 384-well plate. 48 h after transfection, cells were left untreated or stimulated with forskolin alone or forskolin (10 μM) + SDF1α in media containing 100 μM inhibitor of phosphodiesterase, namely isobutylmethylxanthine (3,7-dihydro-1-methyl-3-(2-methylpropyl)-1*H*-purine-2,6-dione), for 15 min at 37 °C and 45 min at room temperature. After an hour of stimulation, lysis buffer alone was added to the untreated cells and lysis buffer with cAMP-d_2 was added to the stimulated cells. Thereafter, cryptate-conjugated cAMP antibody was added to all cells and incubated for 1–2 h. Homogeneous time-resolved fluorescence was recorded with excitation at 320 nm and emission at 620 and 665 nm. A standard curve was prepared by varying the amount of cAMP-d_2 and probing it with cryptate-conjugated cAMP antibody using homogeneous time-resolved fluorescence. The normalized signal from treated cells with respect to untreated cells was converted to the cAMP concentration using the standard curve.

RESULTS

Ca^{2+} Binding to EF Hand Domains of sNUCB1 Induces Conformational Changes—A soluble form of NUCB1 was engineered, expressed in *Escherichia coli,* and purified to homogeneity (Fig. 1*A* and supplemental Fig. S1*A*). The domain architecture of *s*NUCB1 shows two EF hand Ca^{2+}-binding regions sandwiched between an N-terminal DNA binding domain and a C-terminal leucine zipper (20). The thermodynamics of Ca^{2+} binding to *s*NUCB1 were studied using ITC. The Ca^{2+} binding was exothermic with $\Delta H_1^o = -2.1 \pm 0.06$ kcal mol^{-1} and $\Delta S_1^o = 16.5$ cal mol^{-1} K^{-1} for the first EF hand and $\Delta H_2^o = -0.62 \pm 0.31$ kcal mol^{-1} and $\Delta S_2^o = 17.1$ cal mol^{-1} K^{-1} for Ca^{2+} binding to the second EF hand, suggesting a spontaneous uptake of Ca^{2+} by Ca^{2+}-free *s*NUCB1. The recorded data were best fit to a "two-set binding sites" model giving K_d values of 6.3 and 73.5 μM for Ca^{2+} binding (Fig. 1*B*). The difference in binding affinities arises due to the presence of a noncanonical Arg residue substituting for the canonical Gly at the sixth position of the 12-residue Ca^{2+} binding loop of the second EF hand. Our results show that the two EF hands in *s*NUCB1 bind to Ca^{2+} differentially with an order of magnitude difference in their K_d values. In 2004, de Alba and Tjandra (36) heterologously expressed and purified only the EF hand domain (residues 228–326) of NUCB1 and also reported two Ca^{2+}-binding sites with different affinities. The EF hand regions undergo conformational changes upon Ca^{2+} binding that can be monitored through change in *s*NUCB1 Trp fluorescence. *s*NUCB1 has two Trp residues at positions 232 and 333 lying sequentially before and after the EF hand domain, respectively. Steady-state fluorescence measurements show a blue shift of 15 nm and an enhancement in fluorescence intensity as more Ca^{2+} was added to Ca^{2+}-free *s*NUCB1 (supplemental Fig. S1*B*). Thus, Ca^{2+} binding causes a conformational change in *s*NUCB1 causing reorientation of the Trp residues from a solvent-exposed polar to a hydrophobic environment. Fluorescence quenching experiments with acrylamide and iodide were performed to probe the conformational changes around the Trp residues upon Ca^{2+} binding. Acrylamide is a diffusible neutral quencher of Trp fluorescence unaffected by the charges surrounding the fluorophore. I^-, on the other hand, is an anionic quencher for surface-exposed fluorophores only (37). Quenching experiments show that Trp residues are more accessible to acrylamide than I^- for quenching. On binding to Ca^{2+}, acrylamide quenching decreases much more than I^- quenching (supplemental Fig. S1*C*). F_0/F *versus* quencher concentration gave a straight line indicative of a dynamic quenching rather than static quenching. These observations suggest that conformational changes associated with Ca^{2+} binding make Trp residues less accessible by reorienting them into a hydrophobic environment.

The binding of Ca^{2+} to an EF hand motif forms an octahedral coordination sphere, which can cause structural rearrangement in the protein (38). This secondary structural change can in principle be followed by CD spectroscopy. Ca^{2+} binding to *s*NUCB1 causes only a slight increase in helicity. Intriguingly, the far-UV CD spectra of *s*NUCB1 show a smooth structural transition from an α-helical secondary structure at lower concentrations to a predominant β-sheet structure at higher concentrations. These concentration-dependent structural changes were observed both in the absence and presence of Ca^{2+} (supplemental Fig. S2*A*). Furthermore, the thermal unfolding data for *s*NUCB1 showed an increase in apparent T_m of 4 °C on binding to Ca^{2+}. The folding of *s*NUCB1 was observed to be noncooperative and irreversible both in the absence and presence of Ca^{2+} (supplemental Fig. S2*B*). The increase in stabilization on binding to Ca^{2+} suggests a structural ordering of *s*NUCB1.

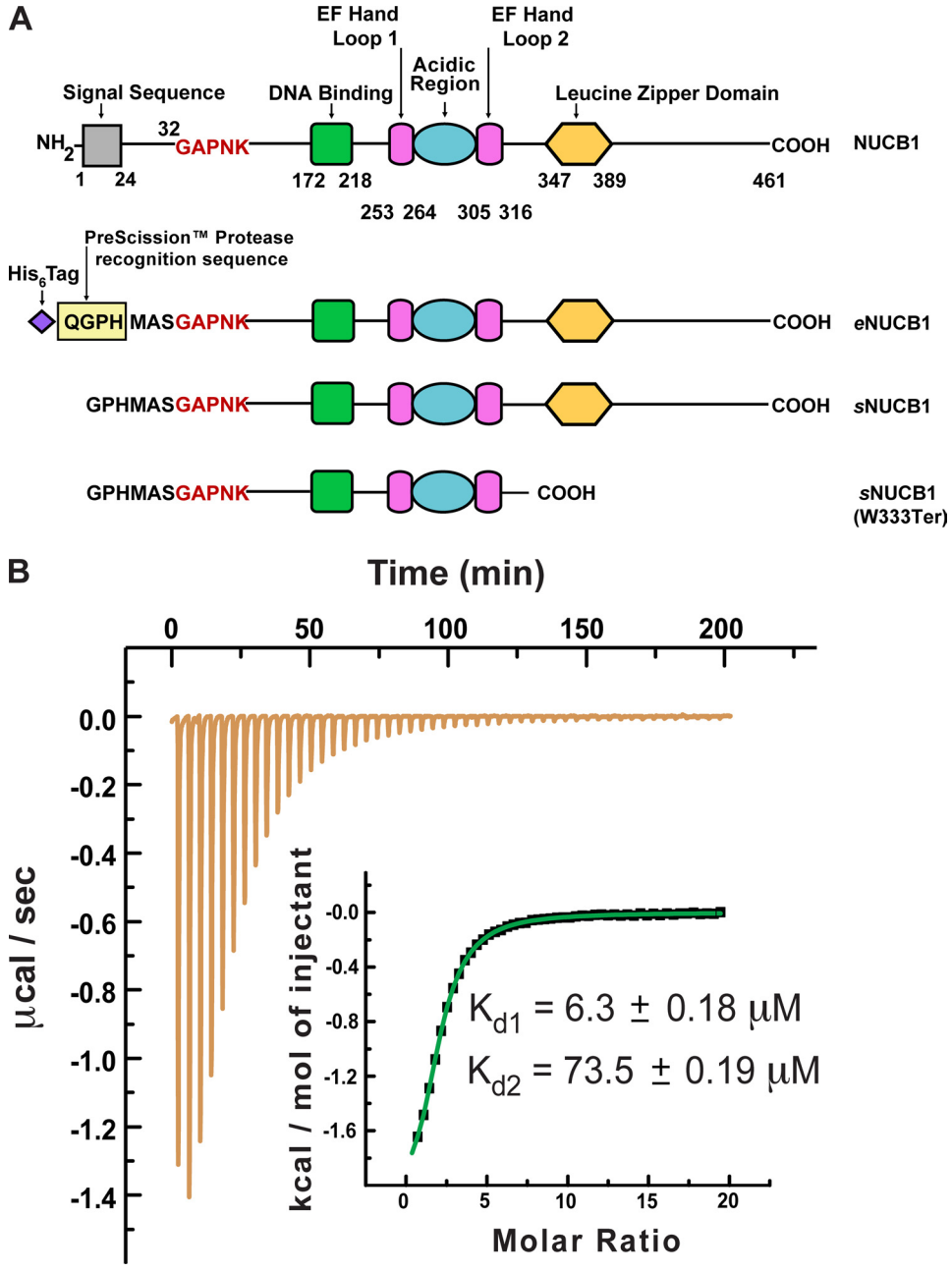

FIGURE 1. **Domain architecture of human NUCB1 and engineered NUCB1 variants and Ca^{2+}-binding activity of a soluble NUCB1 variant.** *A,* modular nature of the NUCB1 protein structure is depicted schematically with its N-terminal signal sequence (*gray square*), putative DNA binding domain (*green square*), two EF hand loops (*magenta rectangles*), acidic region (*blue oval*), and leucine zipper domain (*yellow hexagon*). The amino acid residues at domain borders are *numbered*. We engineered a construct for expression in *E. coli* of a soluble form of NUCB1 that included an N-terminal His_6 tag and a PreScission protease recognition sequence with an intervening spacer sequence as shown. Endoprotease cleavage yields a soluble form of NUCB1 that begins with the amino acid sequence GPHMAS and continues with the remainder of the native sequence beginning at Gly-32. We refer to this expressed protein construct as soluble NUCB1 or *s*NUCB1 throughout the text. We also constructed a double replacement mutant *s*NUCB1(W232A/W333A) and a truncation mutant *s*NUCB1(W333Ter) as shown. *B,* we used isothermal titration calorimetry (*ITC*) to measure the Ca^{2+}-binding affinity of *s*NUCB1. *s*NUCB1 presumably binds one Ca^{2+} cation at each of its two EF hand domains, and a nonlinear least squares fit of the calculated values using the two-set of sites model resulted in an excellent fit as shown in the *inset*. The calculated dissociation constants for Ca^{2+} binding to the two EF hand domains of *s*NUCB1 are 6.3 ± 0.18 and 73.5 ± 0.19 µM, respectively.

NUCB1 Is a Dimer—The domain diagram of NUCB1 reveals the presence of a C-terminal domain leucine zipper, which is a canonical structural motif known to cause dimerization (39). The oligomeric state of NUCB1 was evaluated through sedimentation equilibrium experiments using AUC. This experiment is insensitive to the shape of the molecule and directly reports on the molar mass of the sedimenting species characterized by the Boltzmann distribution. Sedimentation equilibrium measurements were performed with Ca^{2+}-free *s*NUCB1 for concentrations varying from 50 to 150 µM. The data could be well fit to a monomer-*n*-mer model, which gave a molecular mass of ~100 kDa corresponding to a dimer of *s*NUCB1 in solution (Fig. 2*A*). AUC analysis of Ca^{2+}-bound *s*NUCB1 indicated that it is also primarily dimeric in solution (Fig. 2*A*, *inset*). To confirm that the dimerization of *s*NUCB1 is caused by the leucine zipper domain, a C-terminal truncation mutant, *s*NUCB1(W333Ter), lacking the leucine zipper was designed and heterologously expressed. The far-UV CD spectrum of *s*NUCB1(W333Ter) showed an α-helical secondary structure even at high protein concentrations in contrast to the concentration-dependent transition observed for *s*NUCB1 (supplemental Fig. S2*C*). AUC analysis of *s*NUCB1(W333Ter) revealed a monomeric species in solution over the concentration range of 32 to 150 µM (Fig. 2*B*). Similar to *s*NUCB1, the association state of *s*NUCB1(W333Ter) was unaffected upon binding to Ca^{2+} (data not shown). The experiments with the truncation mutant confirm that the leucine zipper domain of *s*NUCB1 is essential for the dimeric state of the protein in solution.

The thermodynamics of the dimerization of *s*NUCB1 was further investigated using MALS. In a series of SEC experiments, Ca^{2+}-free *s*NUCB1 was analyzed by gel filtration using a Superdex200 10/30 HR column. The eluted protein peak was fractionated and subjected to MALS analysis at seven different angles to estimate the molecular mass of the eluting species. As shown in Fig. 2*C*, a gradual increase in the weight-average molecular weight of the eluting species was observed with increasing concentrations of the protein. At concentrations around 10 nM, *s*NUCB1 exists as a monomer. As the concentration is gradually increased, a monomer-dimer equilibrium was

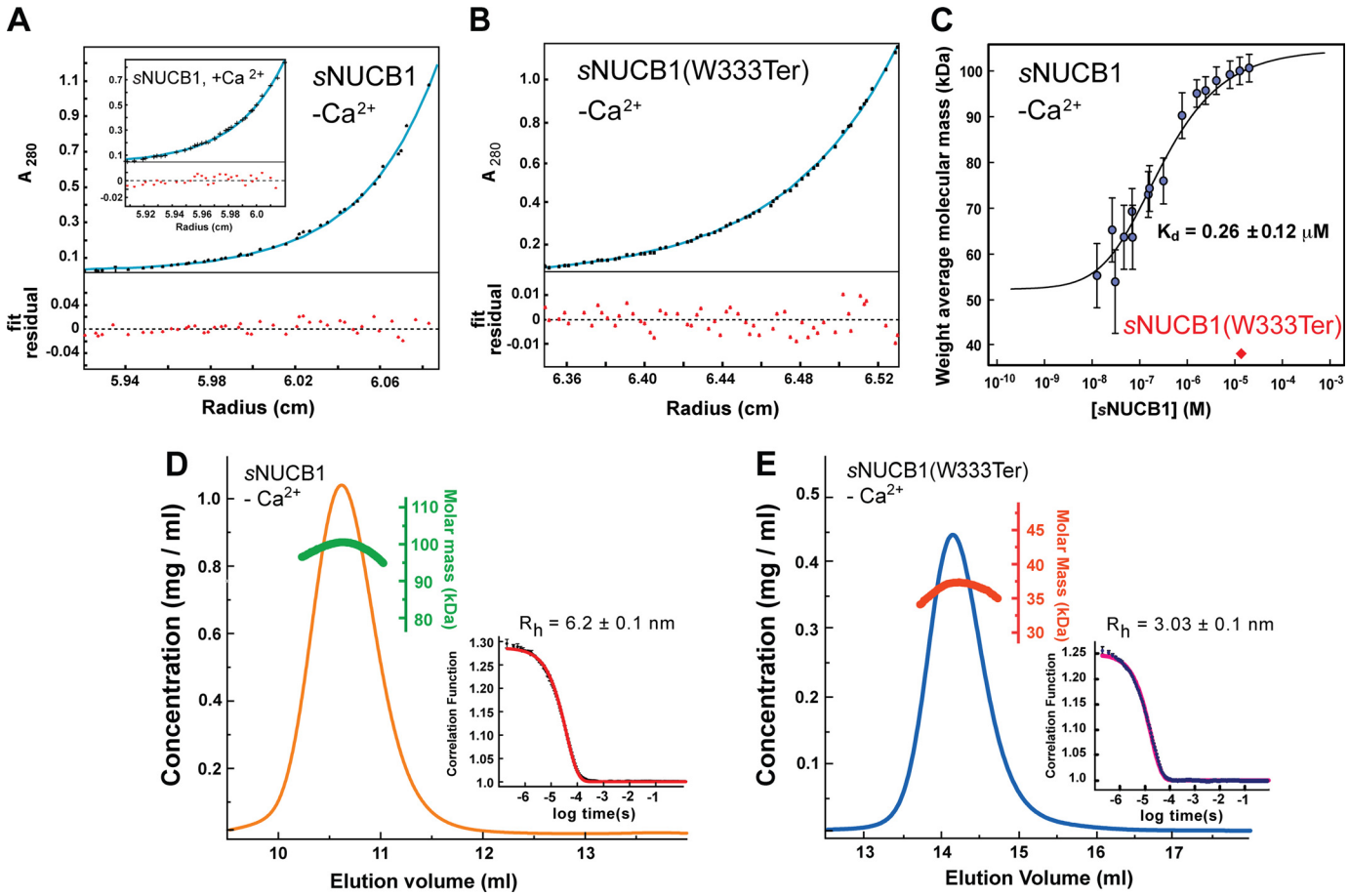

FIGURE 2. ***sNUCB1 forms a stable dimer mediated by its leucine zipper domain.*** *A,* we carried out AUC experiments to determine the oligomeric state of *s*NUCB1 in solution. The sedimentation equilibrium plot for Ca^{2+}-free *s*NUCB1 (50 μM monomeric concentration) shows the evolution of a sample concentration curve resulting from the applied centrifugal force. The data were fit to a monomer-*n*-mer equilibrium model, which gave a measured molecular mass of 98.9 ± 0.41 kDa, consistent with a dimeric structure for *s*NUCB1 in solution (the theoretical molecular mass of monomeric *s*NUCB1 is ~51 kDa). The *inset* shows the sedimentation equilibrium plot for Ca^{2+}-bound *s*NUCB1, which gave essentially an identical molecular mass of 99.4 ± 0.78 kDa. *B,* AUC experiments were carried out on the truncation mutant, *s*NUCB1(W333Ter), which lacked the leucine zipper domain in the C-terminal region of the protein. The AUC sedimentation equilibrium plot for Ca^{2+}-free *s*NUCB1(W333Ter) (70 μM monomeric concentration) gave a molecular mass of 35.2 ± 0.05 kDa, consistent with a monomeric species in solution (the theoretical molecular mass of *s*NUCB1(W333Ter) is ~36.8 kDa). *C,* we studied the monomer-dimer equilibrium of *s*NUCB1 with MALS of fractions with increasing protein concentration collected from Superdex200 10/30 HR size-exclusion chromatography in 50 mM Tris-HCl, pH 8.0, 150 mM NaCl. The weight average molecular weight of the complex at a given protein concentration was determined from a nonlinear least square fit of a collection of values determined for the apex fractions of each eluting peak. A monomer-dimer association model of the values as a function of *s*NUCB1 concentration gave an apparent dissociation constant (K_d) for dimerization of 0.26 ± 0.12 μM. The *error bars* indicate the extent of variation in molecular mass determination originating from the light scattering measurement. We next measured DLS chromatograms for *s*NUCB1 (*D*) and *s*NUCB1(W333Ter) (*E*). Each protein sample was injected onto a Superdex200 10/30 HR column, and the refractive index detector was used to analyze the protein peak. The change in refractive index as a function of protein concentration was used to compute the molecular mass as shown in *green* for *s*NUCB1 and *red* for *s*NUCB1(W333Ter). The molecular mass corresponds to a dimer for *s*NUCB1 and a monomer for *s*NUCB1(W333Ter). The *insets* show the correlation functions as each protein diffuses through the solution in the DLS experiment. The diffusion coefficient from the correlation function gives the hydrodynamic radius (R_h) using Stokes equation. The computed R_h values were 6.2 and 3.03 nm for *s*NUCB1 and *s*NUCB1(W333Ter), respectively.

observed with dimeric *s*NUCB1 dominating at concentrations greater than 1 μM. The data collected at different angles for each run were fit to a monomer-dimer equilibrium model giving a dissociation constant, K_d of dimerization, for *s*NUCB1 of 0.26 ± 0.12 μM. *s*NUCB1(W333Ter) in MALS measurements continued to exist as a monomer even at high protein concentrations. Thus, the leucine zipper region is responsible for the dimeric state of *s*NUCB1 in solution under physiological conditions.

sNUCB1 Is Structurally Asymmetric with an Elongated C Terminus—Ca^{2+}-free *s*NUCB1 in SEC experiments elutes at a much higher volume than a globular protein with a molecular mass similar to that of a *s*NUCB1 monomer or a dimer (supplemental Fig. S3*A*). A plot of the elution parameter, K_{av}, *versus* log(molecular mass) for a number of globular protein standards was utilized to estimate an apparent molecular mass of 300 kDa for *s*NUCB1 (supplemental Fig. S3*B*). This implies that either *s*NUCB1 exists as a trimer of dimers (3× 100 kDa) or is asymmetric in its shape. Because AUC and MALS analysis convincingly ruled out any association of *s*NUCB1 dimers into higher order structures, we proceeded to derive structural information on *s*NUCB1 through DLS. DLS analysis of Ca^{2+}-free *s*NUCB1 yields a hydrodynamic radius (R_h) of 6.2 nm and a frictional coefficient (f/f_0) of 2.03 (Fig. 2*D*). The frictional coefficient of globular proteins usually lies in the range of 1.1–1.25 (40). A value of 2.03 for *s*NUCB1 indicates an asymmetric shape for the dimer, deviating considerably from a sphere. Interestingly, Ca^{2+}-free *s*NUCB1(W333Ter) has an R_h of 3.3 nm and a

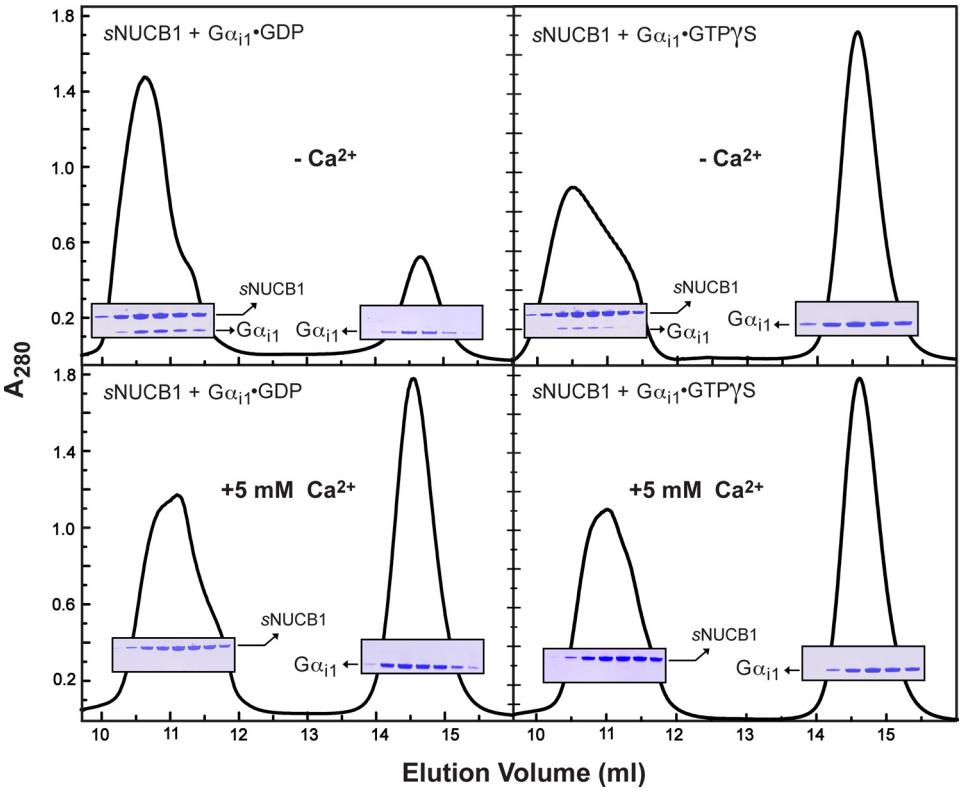

FIGURE 3. ***sNUCB1 forms a stable complex with Gα$_{i1}$•GDP only in the absence of Ca^{2+}.*** We used size-exclusion chromatography to determine the nature of the interaction between *s*NUCB1 and Gα$_{i1}$ in solution under several conditions. *s*NUCB1 and Gα$_{i1}$•GDP were incubated together in the absence (*upper left*) or presence (*lower left*) of Ca^{2+}, and the mixture was subjected to size-exclusion chromatography using a Superdex200 10/30 HR column. Peak fractions were analyzed by SDS-PAGE with Coomassie Brilliant Blue staining as shown in the *insets*. In the absence of Ca^{2+}, *s*NUCB1 and Gα$_{i1}$•GDP formed a complex as judged by the following: (i) the slight shift (from ~11.2 to 10.6 ml) and enhancement of the peak containing only *s*NUCB1 in the presence of Ca^{2+} and both *s*NUCB1 and Gα$_{i1}$ in the absence of Ca^{2+}, and (ii) the depletion, in the absence of Ca^{2+}, of the peak eluting at about 14.6 ml, which contained only Gα$_{i1}$. The same experiment was repeated with *s*NUCB1 and Gα$_{i1}$•GTPγS in the absence (*upper right*) or presence (*lower right*) of Ca^{2+}. Although the same general trend and Ca^{2+} dependence were observed, the apparent ability of Gα$_{i1}$•GTPγS to form a stable complex with *s*NUCB1 was markedly diminished compared with that of Gα$_{i1}$•GDP.

f/f_0 of 1.59 showing that the deletion of the C-terminal domain reduces the radius of hydration by almost 50% (Fig. 2*E*). This suggests that although the N terminus of *s*NUCB1 is relatively more compact and globular, the C-terminal domain of the protein is elongated, contributing to the observed asymmetry in the shape of *s*NUCB1.

sNUCB1 Preferentially Interacts with GDP-bound WT Gα$_{i1}$ in the Absence of Ca^{2+}—NUCB1 is a Ca^{2+}-binding protein that has been shown to interact with G$_i$ and G$_s$ classes of α subunits (16). Physiologically, Gα subunits can individually exist both in the "inactive" or GDP-bound state and the "active" or GTP-bound state. To investigate the interaction of *s*NUCB1 with WT Gα$_{i1}$, *s*NUCB1 was incubated with WT Gα$_{i1}$•GDP (Fig. 3*A*) and WT Gα$_{i1}$•GTPγS (Fig. 3*B*), respectively, and the complex formation was analyzed by SEC using a Superdex200 10/30 HR column. As shown in the *top panels* of Fig. 3, the Coomassie-stained gels of the fractionated peaks show elution of the complex containing both *s*NUCB1 and Gα$_{i1}$ with excess Gα$_{i1}$ fractionating at higher elution volume. The amount of Gα$_{i1}$ eluting with *s*NUCB1 was significantly higher when Gα$_{i1}$ was present in the GDP-bound state rather than in the GTPγS-bound state. Thus, Ca^{2+}-free *s*NUCB1 preferentially interacts with Gα$_{i1}$ in the GDP-bound form. Interestingly, the interaction with Gα$_{i1}$ in both the GDP- and GTPγS-bound states is absent when *s*NUCB1 is bound to Ca^{2+} as shown in the *lower panels* of Fig. 3. The two protein subunits elute out as individual components as the complex is disrupted in the presence of Ca^{2+}. The inhibition of the complex formation between *s*NUCB1 and Gα$_{i1}$ in the presence of Ca^{2+} can be explained by the structural rearrangement of EF hands upon Ca^{2+} binding. Yeast two-hybrid analysis for interaction of Gα with deletion mutants of NUCB1 as bait proposed the EF hand intervening acidic region of NUCB1 to be involved in G protein binding (16). The conformational change induced upon Ca^{2+}-binding can possibly result in the masking of the acidic region sandwiched between the two EF hands, thereby making it inaccessible for G protein binding.

The thermodynamics of Ca^{2+}-free *s*NUCB1 complex formation with Gα$_{i1}$•GDP was investigated using ITC. The exothermic nature of the reaction shows a thermodynamically favorable binding event between the two protein subunits with $\Delta H^0 = -1.45 \pm 0.17$ kcal mol^{-1} and $\Delta S^0 = 16.9$ cal mol^{-1} K^{-1}. The data were best fit to a "one-set binding sites" model with dimeric *s*NUCB1 and monomeric G protein as the interacting partners. The fit provides a K_d value of 18.3 ± 1.45 μM suggesting that *s*NUCB1 interacts relatively weakly with GDP-bound Gα$_{i1}$ (Fig. 4*A*). The association between Ca^{2+}-free *s*NUCB1 and Gα$_{i1}$•GDP was also monitored using light scattering. Protein samples with increasing concentrations of *s*NUCB1-Gα$_{i1}$•GDP complex were injected onto a Superdex200 10/30 HR column, and MALS was done on the complex elution peak. The analysis shows that binding of Gα$_{i1}$•GDP to *s*NUCB1 initiates only after dimerization of Ca^{2+}-free *s*NUCB1. At lower concentrations, dimerization of *s*NUCB1 from molecular mass of 50–00 kDa was traced. Once the dimer was formed, binding of one Gα$_{i1}$•GDP subunit to *s*NUCB1 was evident from an increase in molecular mass to 140 kDa (Fig. 4*B*). The trace observed for *s*NUCB1-Gα$_{i1}$•GDP complex formation can be understood from the experimental K_d values. The K_d value for *s*NUCB1 dimerization is much smaller than the K_d value for binding to Gα$_{i1}$•GDP, resulting in *s*NUCB1 dimerization prior to Gα$_{i1}$•GDP binding. However, *s*NUCB1-Gα$_{i1}$•GDP association curve does not rule out the ability of *s*NUCB1 monomer to interact with Gα$_{i1}$•GDP.

MALS experiments were also conducted with the monomeric truncation mutant *s*NUCB1(W333Ter). A plot of the

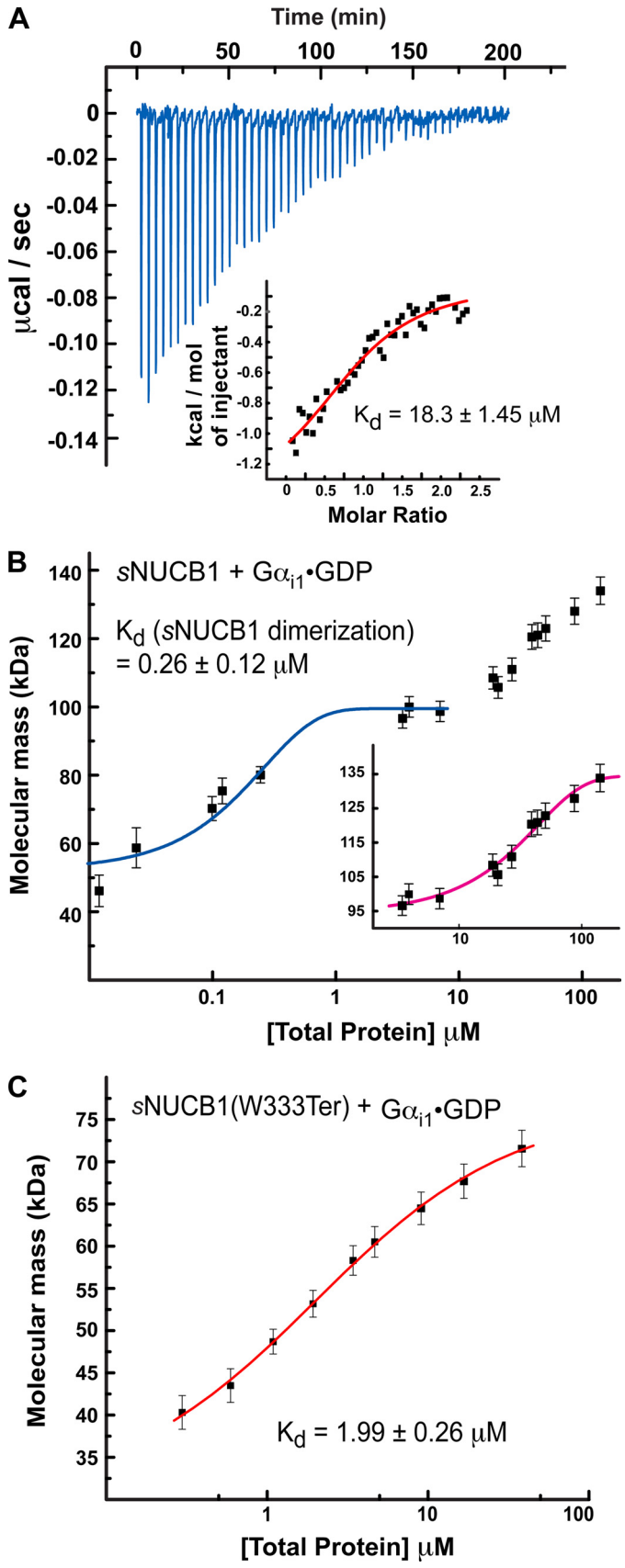

FIGURE 4. **Interaction of *s*NUCB1 and Gα$_{i1}$•GDP.** *A*, we used ITC to measure the binding of Ca^{2+}-free *s*NUCB1 to Gα$_{i1}$•GDP. The heat released per injection of aliquots of a solution of Gα$_{i1}$•GDP (200 μM) into a buffered solution of Ca^{2+}-free *s*NUCB1 (50 μM) was recorded, and the area under the curve was integrated. The heat of dilution for the addition of Gα$_{i1}$•GDP to buffer alone was subtracted. A nonlinear least squares fit of the calculated values using the one-set of sites model for dimeric *s*NUCB1 resulted in a satisfactory fit with a dissociation constant of 18.3 ± 1.45 μM as shown in the *inset*. We used MALS to measure the formation of a complex between *s*NUCB1 and Gα$_{i1}$•GDP (*B*) or the truncation mutant *s*NUCB1(W333Ter) and Gα$_{i1}$•GDP (*C*). MALS data were collected on protein complex peaks eluting from Superdex200 10/30 HR size-exclusion chromatography connected to a high performance liquid chromatography system equipped with an autosampler. Samples with increasing protein concentrations were successively injected onto the column, and the eluate was monitored using a photo-diode UV-visible detector, a differential refractometer, and a static multiangle laser light scattering detector. The weight average molecular weight of the complex was determined as a function of increasing protein concentrations. The *magenta curve* in *B, inset,* and the *red curve* in *C* indicate nonlinear least square fits for a complex formation model of weight average molecular weight values determined for the apex of each eluting peak at various concentrations. The *error bars* indicate extent of variation in molecular mass determination originating from the light-scattering measurement. The data for *s*NUCB1-Gα$_{i1}$•GDP complex formation shows that association between the protein subunits occurs only after dimerization of *s*NUCB1 (*blue curve*). The data suggest that one Gα$_{i1}$ subunit binds to a dimer of *s*NUCB1 and a monomer of *s*NUCB1(W333Ter), respectively, and that the binding site for Gα$_{i1}$ lies in the *s*NUCB1(W333Ter) sequence.

weight average molecular weight obtained from light scattering plotted *versus* the protein concentration shows that monomeric Ca^{2+}-free *s*NUCB1(W333Ter) forms a 1:1 complex with Gα$_{i1}$•GDP. The fit yields a K_d value of 1.99 ± 0.26 μM showing that the interaction of *s*NUCB1 with WT Gα$_{i1}$•GDP becomes stronger on deletion of the C-terminal region of *s*NUCB1 (Fig. 4*C*). This suggests that the C-terminal region of *s*NUCB1 possibly acts as a regulatory domain modulating the interaction of *s*NUCB1 with the G protein α subunit. Alternatively, the structural rearrangement associated with dimerization can also result in the reduced affinity of *s*NUCB1 for Gα$_{i1}$ in comparison with *s*NUCB1(W333Ter).

sNUCB1 Is a GDI—GPCRs activate heterotrimeric G proteins by catalyzing the exchange of GTP for GDP on Gα subunits. The receptor facilitates the nucleotide exchange by using the C-terminally linked α5 helix of Gα subunits. The α5 helix region is postulated to be a molecular microdomain on Gα that allosterically couples the activation signal from the receptor to the catalytic pocket of G proteins (29, 30, 41, 42). Farquhar and co-workers (28) have shown that NUCB1 possibly interacts with the C-terminal α5 helix region of Gα$_{i3}$. We evaluated the effect of this interaction on G protein activation. We measured the nucleotide exchange on Gα in the presence of Ca^{2+}-free *s*NUCB1. The concentrations of both *s*NUCB1 and Gα$_{i1}$ were kept above the determined K_d value for *s*NUCB1-Gα$_{i1}$ complex formation. Steady-state and time-based fluorescence experiments were performed by monitoring the enhancement in Trp fluorescence, which is coupled to activation of Gα$_{i1}$. Any potential contribution from the Trp residues of *s*NUCB1 was eliminated by mutating both Trp-232 and Trp-333 to Ala, thereby generating *s*NUCB1(W232A/W333A) (supplemental Fig. S4*A*). The binding of *s*NUCB1(W232A/W333A) to Gα$_{i1}$•GDP was confirmed using SEC and SDS-PAGE analysis. The interaction of *s*NUCB1(W232A/W333A) with Gα$_{i1}$•GDP was present only in the absence of Ca^{2+} (supplemental Fig. S4*B*). Both AlF_4^- uptake (supplemental Fig. S4*C*) and GTPγS exchange (supplemental Fig. S4*D*) by Gα$_{i1}$•GDP alone shows an increase in Trp fluorescence as Gα$_{i1}$ molecules were acti-

vated with time. However, supplemental Fig. S4, *C* and *D*, shows that binding to *s*NUCB1(W232A/W333A) reduces the relative enhancement of Trp fluorescence coupled to $G\alpha_{i1}$ activation. Furthermore, to simultaneously monitor the activation-associated conformational change in $G\alpha_{i1}$ and the uptake of nucleotide, a mGTPγS-based FRET assay was performed. The binding of mGTPγS in the catalytic pocket of $G\alpha_{i1}$ brings it in close vicinity of Trp-211 on the switch II region of $G\alpha_{i1}$. Hence, FRET can be observed between the Trp and mant fluorophores upon $G\alpha_{i1}$ activation (43). As shown in supplemental Fig. S4*E*, the FRET intensity for $G\alpha_{i1}$ alone at each time point is significantly higher in comparison with the FRET intensity for $G\alpha_{i1}$ associated with Ca^{2+}-free *s*NUCB1(W232A/W333A). These experiments suggest that *s*NUCB1(W232A/W333A) might inhibit nucleotide exchange by $G\alpha_{i1}$.

G protein activation was also monitored using a fluorescent nucleotide analogue BODIPY FL-GTPγS, which absorbs at 504 nm on binding to $G\alpha_{i1}$. We isolated the BODIPY FL-GTPγS-bound fraction of $G\alpha_{i1}$ in the absence and presence of *s*NUCB1 and calculated the amount of bound BODIPY FL-GTPγS in each case (Fig. 5). The supplemental Fig. S5 shows that binding of *s*NUCB1 to $G\alpha_{i1}$ does not affect the λ_{max} of bound BODIPY FL-GTPγS. However, binding of *s*NUCB1 to $G\alpha_{i1}$ reduces the amount of nucleotide exchange by $G\alpha_{i1}$ as seen by a decrease in the BODIPY absorbance. Thus, measuring absorbance of bound BODIPY FL-GTPγS provides a direct monitor of the number of bound nucleotides on $G\alpha_{i1}$ in the presence or absence of *s*NUCB1. Fig. 5*A* shows BODIPY FL-GTPγS nucleotide exchange by $G\alpha_{i1}$ alone (*blue*) and by $G\alpha_{i1}$ in complex with *s*NUCB1 (*orange*). The results show a significant reduction in the number of bound BODIPY FL-GTPγS nucleotides to $G\alpha_{i1}$ when complexed with Ca^{2+}-free *s*NUCB1. This shows that binding of *s*NUCB1 to $G\alpha_{i1}$ causes inhibition of nucleotide exchange.

To further substantiate the effect of *s*NUCB1 on nucleotide exchange by WT $G\alpha_{i1}$, we monitored the exchange of radioligand [^{35}S]GTPγS by $G\alpha_{i1}$ in the presence and absence of *s*NUCB1. Fig. 5*B* shows the kinetics of exchange of GDP for [^{35}S]GTPγS by $G\alpha_{i1}$ alone (*blue*). However, in the presence of *s*NUCB1 (Fig. 5*B*, *green*), the rate and extent of [^{35}S]GTPγS exchange are significantly reduced. Thus, *s*NUCB1 on binding to $G\alpha_{i1}$ influences the nucleotide exchange rate by substantially inhibiting GDP release and subsequently the GTP uptake.

GDI Activity of sNUCB1 Does Not Arise from a Canonical GoLoco Motif—Earlier work by Siderovski and co-workers (9, 14, 44–46) has unraveled several interacting partners of $G\alpha_{i1}$·GDP, namely RGS12, RGS14, AGS3, GPSM2, PCP-2, and G18, all of which possess GDI activity. The GDI activity was attributed to the presence of a single or tandem repeats of a 19-amino acid-long conserved GoLoco motif present in each of these proteins. The crystal structure of $G\alpha_{i1}$·GDP complexed to RGS14-derived GoLoco peptide showed that the conserved C terminus of the 19-amino acid GoLoco motif makes contacts with both the switch I region and the bound nucleotide. Each GoLoco motif ends in a conserved triad of (Asp/Glu)-Gln-Arg. On binding to Gα, the Arg side chain extends into the catalytic pocket to interact directly with the bound GDP and stabilize it. In addition, the highly conserved Asp/Glu and Gln residues are absolutely essential for binding to G protein α subunit as they are involved in both intra- and intermolecular H-bonding interactions (47). A sequence alignment of C-terminal residues of NUCB1(381–399) with GoLoco motifs of several GDIs of $G\alpha_i$ subunits reveals that NUCB1 also possesses the highly conserved triad of Glu-Gln-Arg and the Gln conserved at the 11th position of the GoLoco motifs (supplemental Fig. S6, *A* and *B*). The other residues in the aligned sequence of NUCB1 show relatively poor conservation across the GoLoco motif.

We synthesized the NUCB1 peptide corresponding to residue 381–419, namely NUCB1(381–419) (supplemental Fig. S6*A*). We first performed an ITC experiment to evaluate the interaction of the NUCB1(381–419) with $G\alpha_{i1}$. The supplemental Fig. S6*C* shows that NUCB1(381–419) does not interact with $G\alpha_{i1}$, suggesting that this C-terminal region of NUCB1 alone is not responsible for the observed GDI activity of *s*NUCB1. To identify further the region of *s*NUCB1 responsible for its GDI activity, we tested the effect of C-terminal truncation mutant *s*NUCB1(W333Ter) on the nucleotide exchange by $G\alpha_{i1}$ using [^{35}S]GTPγS exchange assay. Fig. 5*B* illustrates the ability of *s*NUCB1(W333Ter) to inhibit nucleotide exchange on $G\alpha_{i1}$ in a manner similar to *s*NUCB1. This suggests that the GDI activity of *s*NUCB1 lies in the N-terminal part of the protein containing the two EF hands. Thus, the GDI activity of *s*NUCB1 may not depend on a peptide sequence that is similar to a canonical GoLoco sequence.

As a positive control, we also monitored the [^{35}S]GTPγS uptake by $G\alpha_{i1}$ in the presence of RGS14 GoLoco peptide RGS14(496–531). RGS14(496–531) completely inhibits the nucleotide exchange by $G\alpha_{i1}$ (Fig. 5*B*) as reported by Siderovski *et al.* (54). Furthermore, using ITC, we tested the binding of RGS14(496–531) to $G\alpha_{i1}$ both in the absence and presence of *s*NUCB1. As shown in supplemental Fig. S7*A*, RGS14(496–531) (200 μM) binds to $G\alpha_{i1}$ (20 μM) alone with an affinity of 268.8 nM. However, when $G\alpha_{i1}$ was complexed to *s*NUCB1, RGS14(496–531) did not show any binding to $G\alpha_{i1}$ (supplemental Fig. S7*B*) even at a concentration of 500 μM. Similar results were obtained when $G\alpha_{i1}$ was complexed to *s*NUCB1(W333Ter) (supplemental Fig. S7*C*). RGS14(496–531) has been postulated to compete off Gβγ for $G\alpha_i$ binding (47). In our experiments, RGS14(496–531) was not able to bind to $G\alpha_{i1}$ in the presence of *s*NUCB1 suggesting that both RGS14(496–531) and *s*NUCB1 may bind to the same site on $G\alpha_{i1}$. These results demonstrate that the GDI activity of *s*NUCB1 does not originate from the conventional GoLoco motif but that it competes for the same general binding site on $G\alpha_{i1}$.

Physiological Relevance of GDI Activity of sNUCB1—To test the physiological relevance of the observed GDI activity of *s*NUCB1, we expressed the human WT $G\alpha_{i1}$ in the HEK293 cells in the absence and presence of *s*NUCB1. We first measured forskolin-stimulated intracellular cAMP levels for each transfection. Forskolin directly activates adenylyl cyclase (AC), which converts adenosine monophosphate to cAMP. Thus the amount of cAMP production can evaluate the ability of $G\alpha_s$ or $G\alpha_i$ to stimulate or inhibit cellular AC activity. We used the cAMP assay to measure the effect of GDI activity of *s*NUCB1 on

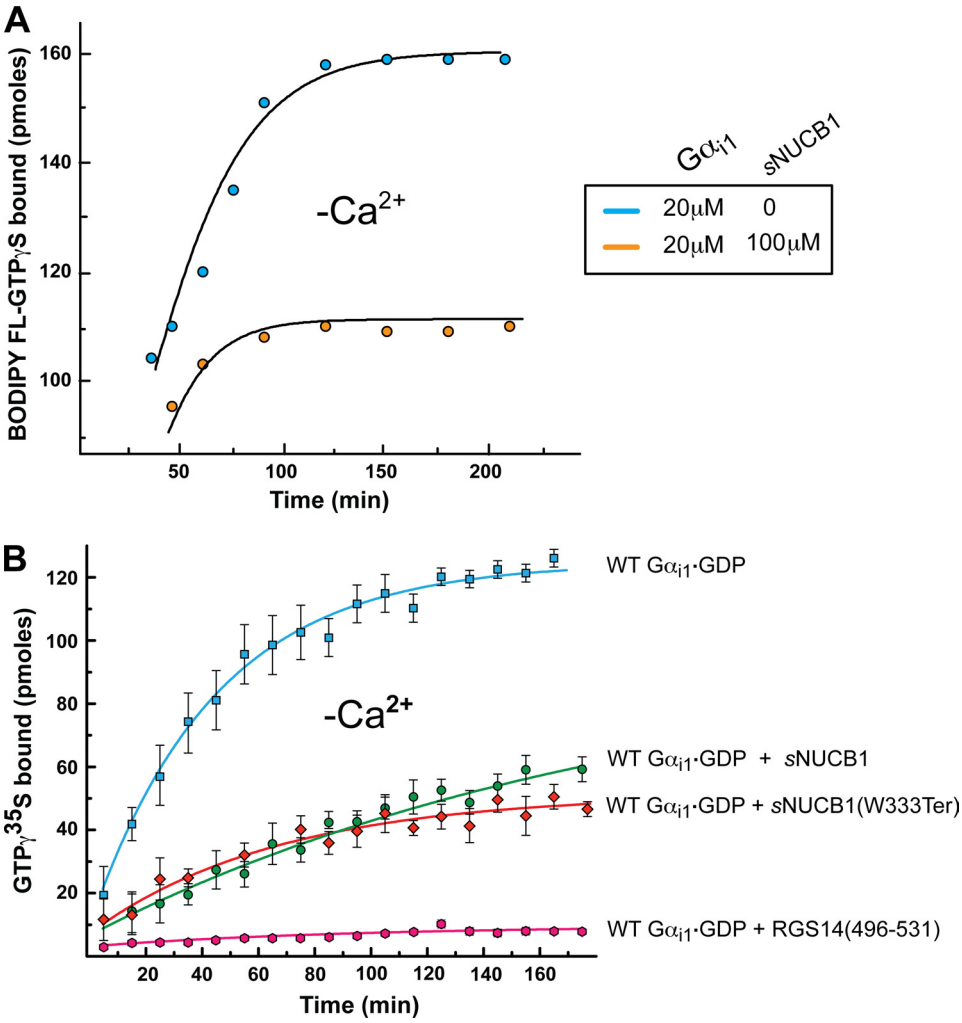

FIGURE 5. **Evidence that *s*NUCB1 acts as a GDI of Gα$_{i1}$.** *A*, we estimated the number of available nucleotide-binding sites on Gα$_{i1}$ in the absence or presence of Ca^{2+}-free *s*NUCB1 by monitoring the absorbance of Gα$_{i1}$-bound BODIPY FL-GTPγS at 504 nm. Gα$_{i1}$·GDP alone (20 μM, *black*) or in complex with Ca^{2+}-free *s*NUCB1 (100 μM, *red*) was allowed to undergo nucleotide exchange with 100 μM BODIPY FL-GTPγS in the reaction mixture. Samples were withdrawn at different time points, and unbound BODIPY FL-GTPγS was removed using a micro-spin desalting column. The amount of bound BODIPY FL-GTPγS was measured using the UV-visible absorbance spectroscopy at each time point. A relative decrease in the number of nucleotide-binding sites on Gα$_{i1}$ was observed on association with *s*NUCB1. This shows that Ca^{2+}-free *s*NUCB1 binds to Gα$_{i1}$ in its GDP-bound form and inhibits nucleotide exchange. We further investigated the guanine nucleotide inhibitory activity of Ca^{2+}-free *s*NUCB1 using the radioligand-based binding assay (*B*). WT Gα$_{i1}$·GDP (20 μM) was incubated alone (*blue*) or with 100 μM Ca^{2+}-free *s*NUCB1 (*green*)/*s*NUCB1(W333Ter) (*red*) in the presence of [^{35}S]GTPγS, and samples were withdrawn at various time points to estimate the amount of radioligand bound upon nucleotide exchange. As a positive control, 100 μM of a C-terminal GoLoco motif peptide from RGS14, namely RGS14(496–531), with established GDI activity was used as a positive control (*magenta*). The data show that both Ca^{2+}-free *s*NUCB1 or Ca^{2+}-free *s*NUCB1(W333Ter) considerably inhibits nucleotide exchange with similar potency. The GDI peptide RGS14(496–531) shows complete inhibition of nucleotide exchange. Each experiment was repeated at least three times, and the data were plotted as mean ± S.E. among the independent measurements.

Gα$_i$ signaling (Fig. 6, *inset*). Intriguingly, the results show that *s*NUCB1 decreases Gα$_i$-mediated AC inhibition after forskolin stimulation.

We further evaluated the effect of *s*NUCB1 on GPCR-mediated signaling. We transfected HEK293 cells with CXCR4 and monitored cAMP production as a function of SDF-1α concentration. SDF-1α is an agonist ligand of CXCR4, which activates the receptor to facilitate nucleotide exchange on Gα$_i$. CXCR4-transfected cells show a dose-response curve for cAMP production upon SDF-1α stimulation with an EC_{50} value of 1 nM. However, when *s*NUCB1 was overexpressed along with CXCR4 and cells were stimulated with SDF-1α, no dose-dependent inhibition was observed. The amount of cAMP produced does not diminish upon stimulation with increasing concentrations of SDF-1α (Fig. 6.).

DISCUSSION

NUCB1 is a ubiquitously expressed multidomain Ca^{2+}-binding protein whose physiological role is not well understood. Our results provide the first direct evidence that *s*NUCB1 is a Ca^{2+}-regulated GDI for Gα$_{i1}$. SEC experiments showed that Ca^{2+}-free *s*NUCB1 interacts primarily with the GDP-bound state of Gα$_{i1}$ and that no interaction occurs when *s*NUCB1 is bound to Ca^{2+} (Fig. 3). The role of Ca^{2+} binding as a regulatory switch for the association of *s*NUCB1 with Gα$_{i1}$ can be explained structurally through the involvement of the acidic region of *s*NUCB1. The acidic region has been previously shown to be a G protein interaction site (28). Thus binding of Ca^{2+} may cause structural rearrangement that can occlude the G protein interaction site on *s*NUCB1. In addition, yeast two-hybrid experiments have suggested that the C-terminally linked α5 helix of G protein interacts with NUCB1 (28). Interestingly, the α5 helix is conformationally identical in both the Gα$_{i1}$·GDP and Gα$_{i1}$·GTPγS structures. However, as Gα undergoes transition from the inactive to the active state, the structurally dynamic switch regions (switch I to IV) of Gα subunits change conformation (48). Thus, the preferential binding of Ca^{2+}-free *s*NUCB1 to Gα$_{i1}$·GDP, which can modulate G protein activation, points toward a possible participation of switch regions in this interaction.

Analysis of the dimer of *s*NUCB1 using SEC (supplemental Fig. S3) and dynamic light scattering (Fig. 2*D*) revealed that it is considerably asymmetric in its shape with a long axis of 12.4 nm. This elongated shape may facilitate simultaneous interaction of *s*NUCB1 with both the α5 helix and the switch regions of Gα$_{i1}$·GDP. Interestingly, deletion of the leucine zipper domain along with the C-terminal region of *s*NUCB1 increased the binding affinity of the monomeric truncation

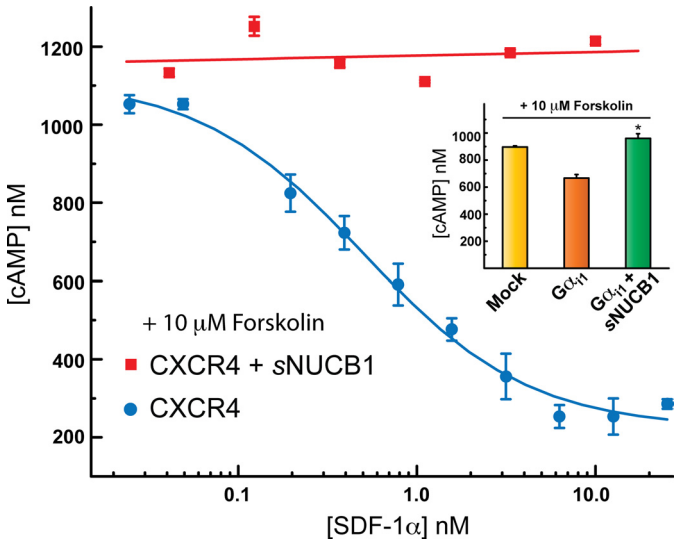

FIGURE 6. ***sNUCB1* overexpression decreases apparent Gα$_{i1}$-dependent inhibition of AC.** The physiological role of interaction of *s*NUCB1 with Gα$_{i1}$ was investigated by monitoring its effect on cellular cAMP production. We transfected HEK293 cells with CXCR4 alone (*blue*) or with *s*NUCB1 and CXCR4 (*red*) cDNA and monitored cAMP production upon ligand (SDF1α)-mediated receptor activation. To increase basal cAMP levels through AC activation at each ligand concentration, cells were stimulated with 10 μM forskolin. For CXCR4 alone (*blue*), we observe significant inhibition of cAMP production upon stimulation with increasing concentrations of receptor agonist ligand. However, upon co-expression of *s*NUCB1 with CXCR4, ligand-dependent receptor-mediated inhibition of cAMP production is markedly reduced (*red*). In the *inset*, we transfected HEK293 cells with mock (*yellow*), Gα$_{i1}$ alone (*orange*), and with *s*NUCB1 and Gα$_{i1}$ (*green*) cDNA, respectively, and then measured cAMP production. The *bar* in *yellow* shows the concentration of cAMP produced with mock transfection, and the *bar* in *orange* shows cAMP production with overexpression of Gα$_{i1}$ alone, and the *bar* in *green* shows cAMP production when *s*NUCB1 was transfected with Gα$_{i1}$. The expression of *s*NUCB1 results in significant enhancement of cAMP production. The results suggest that *s*NUCB1 affects the ability of Gα$_{i1}$ to promote forskolin-stimulated cAMP production by AC; *, $p < 0.05$.

mutant *s*NUCB1(W333Ter) for Gα$_{i1}$·GDP and decreased the R_h to 3.3 nm. This suggests that the deleted C terminus of *s*NUCB1 contributes significantly to the shape asymmetry of *s*NUCB1 and may play a role in regulating *s*NUCB1-Gα$_{i1}$·GDP interaction.

NUCB1 is a major Ca^{2+}-binding protein of Golgi and assists in the uptake, storage, and release of Ca^{2+} from the Golgi apparatus (49). Optimal Golgi Ca^{2+} levels are required for anterograde (endoplasmic reticulum to Golgi), retrograde (Golgi to endoplasmic reticulum), and intra-Golgi transport (50). Thus, NUCB1 along with Cab45 (51), the only other known Ca^{2+}-binding Golgi resident protein, may be involved in maintaining the essential Ca^{2+} levels and gradient from *cis*- to *trans*-Golgi. The Ca^{2+} concentration in *cis*-Golgi is around 0.3 mM under unstimulated conditions (50). Thus, the NUCB1 pool in *cis*-Golgi should largely be Ca^{2+}-bound given the K_d values for Ca^{2+} binding. However, at cytosolic Ca^{2+} concentrations of 100–125 nM (52), NUCB1 should essentially be in a Ca^{2+}-free state. Similar to Gα$_{i1}$, NUCB1 also exists both in the cytosolic and membrane fractions (17), and this creates an opportunity for these two protein subunits to interact and perform physiologically relevant functions. Our ITC experiments along with results from MALS analysis establish the interaction of the Gα$_{i1}$·GDP subunit with a dimer of Ca^{2+}-free *s*NUCB1 (Fig. 4), which is a variant of NUCB1 that lacks the N-terminal signal sequence and represents the cytosolic pool of NUCB1.

Our nucleotide-exchange assays with GTPγS and its fluorescent analogues (supplemental Fig. S4 and supplemental Fig. 5) together show that Ca^{2+}-free *s*NUCB1 significantly inhibits nucleotide exchange by Gα$_{i1}$·GDP. The GDI activity of *s*NUCB1 was established by monitoring exchange of radioligand [^{35}S]GTPγS. Our results clearly show that *s*NUCB1 significantly inhibits Gα$_{i1}$ activation. Interestingly, this ability was unaffected upon deletion of the C-terminal domain of *s*NUCB1, showing that the GDI ability of *s*NUCB1 does not depend on a region of the proteins that resembles a GoLoco motif. Thus, the mechanism of GDI activity of *s*NUCB1 is likely to be different from the GoLoco motif peptides derived from RGS proteins. The RGS peptides generally have nanomolar binding affinity for Gα$_i$·GDP in comparison with micromolar binding affinities observed for GPSM2-, PCP-2-, or G18-derived GoLoco motif peptides (44–46). Unlike these peptide-based studies, our *in vitro* assays report the binding affinity of 18.3 μM for a 99-kDa *s*NUCB1 dimer with Gα$_{i1}$. Yeast two-hybrid analysis by Lin *et al.* (16) showed that NUCB1 preferentially interacts with Gα$_{i1}$ and Gα$_{i3}$ with higher affinity than with Gα$_{i2}$ and Gα$_s$. Further structural studies now underway should reveal the mechanism of GDI activity of *s*NUCB1 and its relevance to other classes of G protein subunits.

G proteins are widely expressed in different tissue types and are involved in various signal transduction pathways interacting with a number of binding partners. The interaction of NUCB1 with Gα$_{i1}$ has been previous established, but no guanine nucleotide exchange factor or GDI activity was observed because the *in vitro* experimental concentrations used were below the K_d values of association. Our results show that *s*NUCB1 inhibits G protein activation and that Ca^{2+} binding regulates interaction of Gα$_{i1}$ with *s*NUCB1. Furthermore, to investigate the physiological importance of this interaction, we performed tissue culture-based experiments. Our results show that upon expression in HEK293 cells, *s*NUCB1 significantly decreases Gα$_i$-mediated AC inhibition. In addition, even receptor-mediated inhibition of AC was prevented by overexpression of *s*NUCB1. This can be explained through the possible sequestration of Gα$_i$ subunits by *s*NUCB1, thereby alleviating inhibition of AC activity. Together with the biophysical studies, this result suggests that *s*NUCB1 and possibly NUCB1 can affect and regulate downstream signaling events involving heterotrimeric G proteins. In 2009, Lin *et al.* (17) showed that NUCB1 affects the dynamic distribution of the Gα subunits to the plasma membrane. It is possible that the association of the two proteins due to colocalization on the secretory granules may facilitate inhibition of G protein activation, which would tend to promote delivery of the Gα protein subunit primarily in the GDP-bound state to the plasma membrane for heterotrimer formation with Gβγ. Thus the cytosolic pool of NUCB1 may exclusively regulate G protein activation, whereas the membrane-bound pool would regulate both the activation and trafficking to facilitate receptor association upon heterotrimer formation.

In addition, NUCB1 also has a nuclear localization signal sequence within the DNA binding region. Recently, its role in

affecting the biogenesis of amyloid precursor protein was reported (27). Such a potential for diverse functionality makes the comprehensive understanding of the physiological role of NUCB1 difficult. Based on our current knowledge, NUCB1 seems to be neither an RGS nor an AGS protein. Future experiments, including structural studies, will unravel the functional relevance of the interaction of NUCB1 with other Gα subunits. Understanding the role of NUCB1 in the context of different Gα subunits will highlight the signaling pathways modulated by NUCB1.

In summary, our results show that *s*NUCB1 is a physiological dimer that interacts with the GDP-bound form of Gα$_{i1}$. The binding of *s*NUCB1 to Gα$_{i1}$ inhibits GDP release and suggests that NUCB1 is a GDI. Ca^{2+} binding to *s*NUCB1 regulates *s*NUCB1-Gα$_{i1}$·GDP complex formation and possibly modulates this interaction in different cellular compartments. We conclude that NUCB1 is a novel Ca^{2+}-binding GDI. The elucidation of the Ca^{2+}-regulated GDI activity of NUCB1 adds a new level of understanding to the role of NUCB1 and to the complexity of G protein-mediated signal regulation.

REFERENCES

1. Oldham, W. M., and Hamm, H. E. (2008) *Nat. Rev. Mol. Cell Biol.* **9,** 60–71
2. Sakmar, T. P., Menon, S. T., Marin, E. P., and Awad, E. S. (2002) *Annu. Rev. Biophys. Biomol. Struct.* **31,** 443–484
3. Gilman, A. G. (1987) *Annu. Rev. Biochem.* **56,** 615–649
4. Pierce, K. L., Premont, R. T., and Lefkowitz, R. J. (2002) *Nat. Rev. Mol. Cell Biol.* **3,** 639–650
5. McCudden, C. R., Hains, M. D., Kimple, R. J., Siderovski, D. P., and Willard, F. S. (2005) *Cell. Mol. Life Sci.* **62,** 551–577
6. Siderovski, D. P., and Willard, F. S. (2005) *Int. J. Biol. Sci.* **1,** 51–66
7. De Vries, L., Zheng, B., Fischer, T., Elenko, E., and Farquhar, M. G. (2000) *Annu. Rev. Pharmacol. Toxicol.* **40,** 235–271
8. Neubig, R. R., and Siderovski, D. P. (2002) *Nat. Rev. Drug Discov.* **1,** 187–197
9. Kimple, R. J., De Vries, L., Tronchère, H., Behe, C. I., Morris, R. A., Gist Farquhar, M., and Siderovski, D. P. (2001) *J. Biol. Chem.* **276,** 29275–29281
10. Willard, F. S., Kimple, R. J., and Siderovski, D. P. (2004) *Annu. Rev. Biochem.* **73,** 925–951
11. Takesono, A., Cismowski, M. J., Ribas, C., Bernard, M., Chung, P., Hazard, S., 3rd, Duzic, E., and Lanier, S. M. (1999) *J. Biol. Chem.* **274,** 33202–33205
12. Blumer, J. B., Cismowski, M. J., Sato, M., and Lanier, S. M. (2005) *Trends Pharmacol. Sci.* **26,** 470–476
13. Kimple, R. J., Willard, F. S., and Siderovski, D. P. (2002) *Mol. Interv.* **2,** 88–100
14. De Vries, L., Fischer, T., Tronchère, H., Brothers, G. M., Strockbine, B., Siderovski, D. P., and Farquhar, M. G. (2000) *Proc. Natl. Acad. Sci. U.S.A.* **97,** 14364–14369
15. Mochizuki, N., Hibi, M., Kanai, Y., and Insel, P. A. (1995) *FEBS Lett.* **373,** 155–158
16. Lin, P., Le-Niculescu, H., Hofmeister, R., McCaffery, J. M., Jin, M., Hennemann, H., McQuistan, T., De Vries, L., and Farquhar, M. G. (1998) *J. Cell Biol.* **141,** 1515–1527
17. Lin, P., Fischer, T., Lavoie, C., Huang, H., and Farquhar, M. G. (2009) *Mol. Neurodegener.* **4,** 15
18. Kanai, Y., and Tanuma, S. (1992) *Immunol. Lett.* **32,** 43–48
19. Miura, K., Titani, K., Kurosawa, Y., and Kanai, Y. (1992) *Biochem. Biophys. Res. Commun.* **187,** 375–380
20. Miura, K., Kurosawa, Y., and Kanai, Y. (1994) *Biochem. Biophys. Res. Commun.* **199,** 1388–1393
21. Kanuru, M., Samuel, J. J., Balivada, L. M., and Aradhyam, G. K. (2009) *FEBS J.* **276,** 2529–2546
22. Lavoie, C., Meerloo, T., Lin, P., and Farquhar, M. G. (2002) *Mol. Endocrinol.* **16,** 2462–2474
23. Wang, S. N., Miyauchi, M., Koshikawa, N., Maruyama, K., Kubota, T., Miura, K., Kurosawa, Y., Awaya, A., and Kanai, Y. (1994) *Pathol. Int.* **44,** 844–849
24. Tsukumo, Y., Tsukahara, S., Saito, S., Tsuruo, T., and Tomida, A. (2009) *J. Biol. Chem.* **284,** 27500–27510
25. Leclerc, P., Biarc, J., St-Onge, M., Gilbert, C., Dussault, A. A., Laflamme, C., and Pouliot, M. (2008) *PLoS One* **3,** e2229
26. Brodeur, J., Larkin, H., Boucher, R., Thériault, C., St-Louis, S. C., Gagnon, H., and Lavoie, C. (2009) *Traffic* **10,** 1098–1114
27. Lin, P., Li, F., Zhang, Y. W., Huang, H., Tong, G., Farquhar, M. G., and Xu, H. (2007) *J. Neurochem.* **100,** 1505–1514
28. Lin, P., Fischer, T., Weiss, T., and Farquhar, M. G. (2000) *Proc. Natl. Acad. Sci. U.S.A.* **97,** 674–679
29. Kapoor, N., Menon, S. T., Chauhan, R., Sachdev, P., and Sakmar, T. P. (2009) *J. Mol. Biol.* **393,** 882–897
30. Marin, E. P., Krishna, A. G., and Sakmar, T. P. (2001) *J. Biol. Chem.* **276,** 27400–27405
31. Marin, E. P., Krishna, A. G., and Sakmar, T. P. (2002) *Biochemistry* **41,** 6988–6994
32. Folta-Stogniew, E., and Williams, K. R. (1999) *J. Biomol. Tech.* **10,** 51–63
33. Koppel, D. E. (1972) *J. Chem. Phys.* **57,** 4814
34. Cummins, P. G., and Staples, E. J. (1981) *J. Physics E-Scientific Instruments* **14,** 1171–1177
35. Vanholde, K. E., and Baldwin, R. L. (1958) *J. Phys. Chem.* **62,** 734–743
36. de Alba, E., and Tjandra, N. (2004) *Biochemistry* **43,** 10039–10049
37. Phillips, S. R., Wilson, L. J., and Borkman, R. F. (1986) *Curr. Eye Res.* **5,** 611–619
38. Cates, M. S., Berry, M. B., Ho, E. L., Li, Q., Potter, J. D., and Phillips, G. N., Jr. (1999) *Structure* **7,** 1269–1278
39. Landschulz, W. H., Johnson, P. F., and McKnight, S. L. (1988) *Science* **240,** 1759–1764
40. Siegel, L. M., and Monty, K. J. (1966) *Biochim. Biophys. Acta* **112,** 346–362
41. Natochin, M., Moussaif, M., and Artemyev, N. O. (2001) *J. Neurochem.* **77,** 202–210
42. Oldham, W. M., Van Eps, N., Preininger, A. M., Hubbell, W. L., and Hamm, H. E. (2006) *Nat. Struct. Mol. Biol.* **13,** 772–777
43. Willard, F. S., Kimple, R. J., Kimple, A. J., Johnston, C. A., and Siderovski, D. P. (2004) *Methods Enzymol.* **389,** 56–71
44. Willard, F. S., McCudden, C. R., and Siderovski, D. P. (2006) *Cell. Signal.* **18,** 1226–1234
45. McCudden, C. R., Willard, F. S., Kimple, R. J., Johnston, C. A., Hains, M. D., Jones, M. B., and Siderovski, D. P. (2005) *Biochim. Biophys. Acta* **1745,** 254–264
46. Kimple, R. J., Willard, F. S., Hains, M. D., Jones, M. B., Nweke, G. K., and Siderovski, D. P. (2004) *Biochem. J.* **378,** 801–808
47. Kimple, R. J., Kimple, M. E., Betts, L., Sondek, J., and Siderovski, D. P. (2002) *Nature* **416,** 878–881
48. Mixon, M. B., Lee, E., Coleman, D. E., Berghuis, A. M., Gilman, A. G., and Sprang, S. R. (1995) *Science* **270,** 954–960
49. Lin, P., Yao, Y., Hofmeister, R., Tsien, R. Y., and Farquhar, M. G. (1999) *J. Cell Biol.* **145,** 279–289
50. Pezzati, R., Bossi, M., Podini, P., Meldolesi, J., and Grohovaz, F. (1997) *Mol. Biol. Cell* **8,** 1501–1512
51. Scherer, P. E., Lederkremer, G. Z., Williams, S., Fogliano, M., Baldini, G., and Lodish, H. F. (1996) *J. Cell Biol.* **133,** 257–268
52. Usachev, Y. M., Marchenko, S. M., and Sage, S. O. (1995) *J. Physiol.* **489,** 309–317